Variations of Li and Mg isotope ratios in bulk chondrites and mantle xenoliths

Philip A.E. Pogge von Strandmann[1], Tim Elliott[1], Horst R. Marschall[1,2], Chris Coath[1], Yi-Jen Lai[1], Alistair B. Jeffcoate[1], Dmitri A. Ionov[3]

[1]Bristol Isotope Group, Department of Earth Sciences, Bristol University, Wills Memorial Building, UK

[2]Department of Geology and Geophysics, Woods Hole Oceanographic Institute, Woods Hole, MA 02543, USA

[3] Universite de Lyon, UJM Saint Etienne & UMR6524-CNRS "Magmas et Volcans", 42023 cedex 02 Saint Etienne, France

Abstract

We present whole rock Li and Mg isotope analyses of 33 ultramafic xenoliths from the terrestrial mantle, which we compare with analyses of 30 (mostly chondritic) meteorites. The accuracy of our new Mg isotope ratio measurement protocol is substantiated by a combination of standard addition experiments, the absence of mass independent effects in terrestrial samples and our obtaining identical values for rock standards using 2 different separation chemistries and 3 different mass-spectrometric introduction systems. Carbonaceous, ordinary and enstatite chondrites have irresolvable mean stable Mg isotopic compositions (δ^{25}Mg = -0.14 ± 0.06; δ^{26}Mg = -0.27 ± 0.12‰, 2sd), but our enstatite chondrite samples have lighter δ^{7}Li (by up to ~3‰) than our mean carbonaceous and ordinary chondrites (3.0 ± 1.5‰, 2sd), possibly as a result of spallation in the early solar system. Measurements of equilibrated, fertile peridotites give mean values of δ^{7}Li = 3.5 ± 0.5‰, δ^{25}Mg = -0.10 ± 0.03‰ and δ^{26}Mg = -0.21 ± 0.07‰. We believe these values provide a useful estimate of the primitive mantle and they are within error of our average of bulk carbonaceous and ordinary chondrites. A fuller range of fresh, terrestrial, ultramafic samples, covering a variety of geological histories, show a broad positive correlation between bulk δ^{7}Li and δ^{26}Mg, which vary from -3.7 to +14.5‰, and -0.36 to +0.06‰, respectively. Values of δ^{7}Li and δ^{26}Mg lower than our estimate of primitive mantle are strongly linked to kinetic isotope fractionation, occurring during transport of the mantle xenoliths. We suggest Mg and Li diffusion into the xenoliths is coupled to H

loss from nominally anhydrous minerals following degassing. Diffusion models suggest that the co-variation of Mg and Li isotopes requires comparable diffusivities of Li and Mg in olivine. The isotopically lightest samples require ~5-10 years of diffusive ingress, which we interpret as a time since volatile loss in the host magma. Xenoliths erupted in pyroclastic flows appear to have retained their mantle isotope ratios, likely as a result of little prior degassing in these explosive events. High δ^7Li, coupled with high [Li], in rapidly cooled arc peridotites may indicate that these samples represent fragments of mantle wedge that has been metasomatised by heavy, slab-derived fluids. If such material is typically stirred back into the convecting mantle, it may account for the heavy δ^7Li seen in some oceanic basalts.

1.0 Introduction

New stable isotopic tracers provide novel means to assess the composition of the mantle, its relationship to meteoritic building blocks and processes that cause heterogeneity. Both lithium (^{6}Li and ^{7}Li) and magnesium (^{24}Mg, ^{25}Mg and ^{26}Mg) isotopes have received considerable recent interest e.g. (Tomascak, 2004; Young and Galy, 2004), the former for its potential to trace recycled material e.g. (Elliott et al., 2004), and the latter as a major constituent of the mantle. There are some notable similarities in the elemental and isotopic behaviour of Li and Mg which make it worthwhile to consider these tracers jointly. Lithium readily substitutes for Mg in many mineral structures, having a comparable ionic radius (Shannon and Prewitt, 1969). Notably, Li and Mg are both largely hosted in olivine in the shallow mantle. Cosmochemically, Mg and Li are only moderately volatile and so the isotopic composition of meteorites should usefully inform on the bulk composition of the Earth e.g. (Palme and O'Neill, 2003). The large relative mass differences between ^{7}Li-^{6}Li and ^{26}Mg-^{24}Mg result in considerable variability in δ^7Li and δ^{26}Mg in the low-temperature silicate weathering environment e.g. (Chan et al., 1992; Tipper et al., 2006b), but the relatively high diffusivities of Li (Svanson and Johansson, 1970; Jambon et al., 1978; Lowry et al., 1982) and to a lesser extent Mg (Morioka, 1981; Chakraborty et al., 1994) can result in their diffusive isotopic fractionation at magmatic temperatures (Richter et al., 2003; Lundstrom et al., 2005; Teng et al., 2006; Richter et al., 2008).

Here we make a coupled Li and Mg isotopic study of magma-hosted, ultramafic xenoliths. An impetus for this combination is to use Mg to help better understand the importance of diffusive fractionations in the Li isotopic composition of mantle-derived samples. Although the role of diffusive fractionation of Li during entrainment, transport and eruption of xenoliths is well documented, especially at the mineral scale (Jeffcoate et al., 2007; Rudnick and Ionov, 2007; Tang et al., 2007; Ionov and Seitz, 2008; Kaliwoda et al., 2008), its importance in influencing bulk xenolith compositions is less clear. Moreover, it is anticipated that deep recycling of surface materials might create primary differences in δ^7Li within the mantle, as has been inferred from the Li isotopic compositions of some oceanic basalts (Chan and Frey, 2003; Ryan and Kyle, 2004; Nishio et al., 2005; Elliott et al., 2006; Chan et al., 2009). Thus it would be useful to be able to distinguish primary variability from recent diffusive fractionation. Mg offers the potential to clarify this ambiguity. As the major mantle cation, addition of recycled material will have minimal effect on its isotopic ratio, whereas diffusive processes will likely fractionate Mg together with Li (Richter et al., 2003; Richter et al., 2008). Hence we have analysed whole rock Li and Mg isotopic ratios on a range of xenoliths, including samples in which variable amounts of diffusive fractionation have already been identified (Jeffcoate et al., 2007; Rudnick and Ionov, 2007), a suite of xenoliths from a mantle wedge setting that might display primary heavy Li isotope signatures and additional samples that have experienced a range of metasomatic enrichment processes.

In order to identify perturbation of Li and Mg isotope ratios from either recycling or diffusion, it is necessary to establish a reference for the primitive mantle. Thus we have also analysed a range of chondritic meteorites. Given the recent profusion of not always consistent Mg isotopic data for mantle-derived samples (Norman et al., 2006; Pearson et al., 2006; Teng et al., 2007; Wiechert and Halliday, 2007; Handler et al., 2009; Huang et al., 2009a; Yang et al., 2009; Bourdon et al., 2010; Chakrabarti and Jacobsen, 2010; Teng et al., 2010; Bizzarro et al., 2011; Huang et al., 2011) we have also made some effort to assess the accuracy of Mg isotopic measurements by using several different approaches.

2.0 Samples

We have largely focussed on whole-rock samples in order to obtain representative bulk compositions. Studies of traditional, radiogenic, highly

incompatible isotope tracers have noted that element budgets hosted along grain boundaries can have a major influence on bulk xenolith compositions (Zindler and Jagoutz, 1988) and so have typically focussed on analysing individual mineral phases. Such problems should not be a concern for a compatible element like Mg, or even a moderately incompatible one like Li, for which an overwhelming fraction of the element is hosted in the major mineral phases. Moreover, the assumption for radiogenic isotopic systems that the composition of one phase can represent the bulk is less robust for stable isotopic systems (e.g. Li, Mg, Ca), in which there might be significant intra-mineral equilibrium fractionation (Seitz et al., 2004; Young et al., 2009; Huang et al., 2010b; Li et al., 2011). In the case of Li, it can be also difficult to reconstitute bulk compositions from individual mineral analyses of highly isotopically zoned constituent minerals (Jeffcoate et al., 2007).

Well-characterised, ultramafic xenoliths from several different geodynamic settings, with variable histories of enrichment and depletion were analysed. Figure 1 illustrates the variability in melt depletion and metasomatism experienced by different sample suites, as indicated by Mg# and primitive mantle normalised La/Sm (McDonough and Frey, 1989; Workman and Hart, 2005). Many of the samples in this study have also been analysed for Fe isotopes by Weyer and Ionov (2007). Our samples include xenoliths hosted in the Cenozoic alkali basalts from Tok in the SE Siberian craton (Ionov et al., 2005b; Ionov et al., 2005c; Ionov et al., 2006), from off-craton sites in central Asia (Preß et al., 1986; Ionov and Wood, 1992; Ionov, 2004; Ionov et al., 2005a; Ionov, 2007; Ionov and Hofmann, 2007), and xenoliths from the Avacha andesitic volcano in Kamchatka (Weyer and Ionov, 2007; Ionov and Seitz, 2008; Ionov, 2010). Brief overviews of the xenolith localities are provided below.

The cratonic Tok xenoliths represent two different groups: lherzolite-harzburgite (LH), comprising fertile to highly refractory peridotite, and lherzolite-wehrlite (LW) groups, where complete or large-scale replacement of orthopyroxene by clinopyroxene has occurred (Ionov et al., 2005b; Ionov et al., 2005c; Ionov et al., 2006; Rudnick and Ionov, 2007). The LH group reflects variable amounts of melt extraction at shallow levels from a fertile source. Refractory LH peridotites (olivine-rich, cpx-poor) are strongly metasomatised, probably by several metasomatic stages (first by percolation of evolved fluids, then by alkali-rich fluids) and tend to be relatively enriched in the LREE (Fig. 1). The associated lherzolite-wehrlite (LW) group was formed by the reaction of refractory residual peridotite (i.e. the LH series

protolith) with evolved Fe-rich silicate liquids and are characterised by complete or large-scale replacement of orthopyroxene by clinopyroxene and low Mg# (<0.89) (Ionov et al., 2005b, Ionov et al., 2005c; Ionov et al., 2006; Rudnick and Ionov, 2007). Unlike most of the other samples (below), xenoliths from the Tok locality are typically hosted in lava flows rather than pyroclastic eruptions (Table 1).

Off-craton xenoliths are represented by samples from Tariat (Ionov, 2007; Ionov and Hofmann, 2007) and Dariganga (Wiechert et al., 1997) in Mongolia, and Vitim in southern Siberia (Ionov, 2004; Ionov et al., 2005a). These samples generally comprise fertile spinel and garnet lherzolites, which are uncommon in global occurrence, and some spinel harzburgites, some of which have been variably metasomatised. The Mongolian (Tariat) peridotite xenoliths are fertile spinel lherzolites and spinel harzburgites, some of which have also been variably metasomatised. Metasomatic processes include Fe-enrichment through chemical exchange between the host peridotite and percolating Fe-rich melt with no significant phase reactions. Prior to metasomatism, these samples were probably fairly fertile peridotites depleted by generally low-degree but variable melt extraction, and some samples (Mo-101) retain their fertile character (Ionov, 2007; Ionov and Hofmann, 2007; Wichert et al., 1997). Vitim is represented by fertile spinel and garnet lherzolites, erupted in picritic tuffs. These samples are thought to reflect moderate degrees of melt extraction from a fertile protolith, similar in composition to the primitive mantle, and have been little affected by modal or cryptic metasomatism (Ionov, 2004; Ionov et al., 2005a).

The spinel harzburgites from Avacha (Kamchatka) provide examples of arc peridotites, situated ~120km above the subducting Pacific plate (Gorbatov et al., 1997). They are thus interpreted as direct samples of mantle wedge regions affected by melt extraction and upward fluid migration from the slab (Ionov and Seitz, 2008). The samples studied here were selected on a basis of the absence of reaction with their host magmas (i.e. they contain no macroscopically detectable veins or modal heterogeneities) and any post-eruptive alteration (Ionov, 2010). The Avacha xenoliths were erupted in rapidly cooling pyroclastic cinder (Ionov, 2010).

Although samples were dominantly selected to record a wide range of possible mantle processes, we also chose a small sub-set of fertile upper mantle compositions likely to be representative of the convecting mantle (Fig. 1). In order for these samples to be a useful, primary reference for Li isotopes, we wished to avoid

xenoliths that had experienced diffusive Li isotope fractionation during entrainment and emplacement (Jeffcoate et al., 2007; Rudnick and Ionov, 2007; Tang et al., 2007; Ionov and Seitz, 2008; Kaliwoda et al., 2008). Thus we chose four fertile samples (Mo-101, 314-56, 313-102, 314-58), for which previous analyses of co-existing mineral phases indicated minimal diffusive disturbance of Li (Magna et al., 2006b; Jeffcoate et al., 2007).

In order to provide a meteoritic reference against which to gauge terrestrial mantle variability, we analysed a total of 30 bulk meteorite samples of different groups and metamorphic grades (see Table 1 for details). We focussed on undifferentiated meteorites, as possible representatives of bulk planetary compositions, including 9 carbonaceous chondrites, 10 ordinary and 7 enstatite chondrites. We additionally analysed a few differentiated meteorites (3 eucrites and an aubrite) for Li isotopes.

3.0 Methods

3.1 Chemistry

Powdered samples were dissolved in concentrated HF-HNO_3-$HClO_4$, followed by stages of concentrated (~15M) HNO_3 and 6M HCl. $HClO_4$ was primarily used to prevent the formation of insoluble Li-fluorides (Ryan and Langmuir, 1987). Mineral separates and chondrite chips were first cleaned by ultrasonication in methanol and MQ H_2O; all samples for Li isotope analysis were then crushed, whereas whole crystals were dissolved without prior crushing for Mg isotope measurements, because the small amount of material required made this possible. Li concentrations, if not already available, were measured on an Element 2 ICP-MS (inductively coupled plasma mass spectrometer) using a calibration line comprising standards JP-1 ([Li]=1.66μg/g), BHVO-2 (4.42μg/g) and BCR-2 (8.63μg/g), whose concentrations were determined by isotope dilution using a 95% enriched ^{6}Li spike, which had been calibrated against a gravimetric L-SVEC solution. JB-2 was analysed as an unknown in every run and yielded [Li] = 7.43±0.38μg/g.

For each sample, ~10ng of Li were purified by a two-step cation column (AG50W X12) separation method using dilute HCl as an eluant, as described elsewhere (James and Palmer, 2000; Marschall et al., 2007b). ~1μg of Mg was separated from a different split of the same dissolution. The sample matrix was also

removed with a two-step cation exchange (AG 50W X12) high aspect ratio column method using a 2.0N HNO_3 eluant (Lee and Papanastassiou, 1974; Lee et al., 1976; Black et al., 2006; Teng et al., 2007; Huang et al., 2009b). 2.4ml dry volume of resin was used for the first column (Pogge von Strandmann, 2008), and 0.25ml for the second column (Foster et al., 2010). The effectiveness of chemical separation using these procedures was determined by ICP-MS for several rock standards. The post-chemistry Mg/Al mass ratios in the JP-1 peridotite were >1000 and Mg/Mn > 1100, whilst Fe and Ca were below detection limits. For BHVO-2 basalt, Mg/Al > 400, Mg/Fe > 800 and Ca and Mn were below detection limits. Mg/cation ratios <20 are thought to cause analytical artefacts (Galy et al., 2001; Teng et al., 2007), and this methodology clearly betters this threshold by at least an order of magnitude. Contributors to spectral interferences on Mg ($^{48}Ti^{++}$, $^{50}V^{++}$, $^{52}Cr^{++}$) are also effectively removed by the chemistry ($^{24}Mg/^{48}Ti > 8000$; $^{25}Mg/^{50}V > 5000$; $^{26}Mg/^{52}Cr > 1000$), bearing in mind that the doubly charged ions will be orders of magnitude less abundant in the ion source than singly charged species. Both Li and Mg isotopes fractionate during cation chromatography, and therefore it is essential to have column yields close to 100%. To assess this, splits of the elution were collected before and after the collection bracket for Li or Mg, and were analysed for Li or Mg content. This showed that <0.1% of Li and Mg were present in these splits.

To compare the HNO_3-based purification method for Mg to the alternative HCl method (Chang et al., 2003; Tipper et al., 2006a; Wiechert and Halliday, 2007; Tipper et al., 2008), several rock standards were first purified through anion exchange resin (AG1 X8) using 6M HCl to remove elements such as Fe (as Fe elutes contemporaneously to Mg in cation exchange resin when using HCl), before being passed though the same cation exchange columns detailed above using dilute (1.75N) HCl. In JP-1 thus purified, Mg/Fe > 3000, Mg/Al > 75 and Mg/Ca > 200. Purified BHVO-2 has Mg/Al > 100, Mg/Fe > 1000 and Mg/Ca >200. This suggests that although the HCl method is marginally more efficient in removing Fe due to the initial anionic resin step, the HNO_3 method removes the rest of the major matrix elements more effectively. However both procedures are capable of removing matrix sufficiently well for analysis. The results of rock standards processed using both methods are discussed below.

The minor element Ni is not efficiently removed from Mg by either chemical separation procedure. The Mg/Ni ratios of different mantle and mantle-derived

samples can vary considerably and so analysed solutions may also have quite variable Mg/Ni (Mg/Ni of JP-1 and BHVO-2 purified using HNO_3 are ~200 and ~1000, respectively). Thus we tested the effects of different Mg/Ni on analysed solutions by doping the DSM-3 standard (Galy et al., 2003). No isotopic variability was measured down to Mg/Ni ratios of 1 (Fig. 2). A similar finding was reported by Teng et al., 2010 for "wet" plasma (see Section 3.2), but both Teng et al., 2010 and Huang et al., 2009 reported resolvable δ^{26}Mg variation when Ni doping with "dry" desolvation plasma. This may indicate that desolvation techniques are more susceptible to matrix effects, and is discussed below. The total procedural blank for Mg isotope analysis using HNO_3 is ~0.4ng which is insignificant compared to the mass of sample used.

3.2 Mass spectrometry

Li isotope measurements were performed on a Thermo-Finnigan Neptune multi-collector inductively coupled plasma mass-spectrometer (MC-ICP-MS), as detailed elsewhere (Jeffcoate et al., 2004). Prior to analysis, the Na/Li intensity ratio was measured, as ratios >3 can cause inaccurate analyses. If samples had higher Na/Li ratios, they were re-purified. This occurred in approximately 1 in 50 samples. Multiple analyses of several international rock standards over a period of four years (Table 2) yielded a $2\sigma_{SD}$ external reproducibility of ±0.3‰, in keeping with previously cited reproducibility (Elliott et al., 2006; Jeffcoate et al., 2007). Results are presented as δ^7Li, namely the ‰ deviations from the standard L-SVEC (Flesch, 1973).

Magnesium isotope analyses were also made on a Neptune using high sensitivity "X" Ni skimmer cones. Prior to measurement, the intensities of Na, Al, Ca, Ti and Fe were checked on the Neptune to ensure that the matrix was consistently removed, but a high residual matrix was never observed. A sample-standard bracketing technique was used, relative to the standard DSM-3 (Galy et al., 2003). Each sample was measured four separate times during an analytical procedure, repeat measurements being separated by several hours, but during the same analysis session. Each individual measurement consisted of 20 ratios (84s total integration time), giving a total integration time of 336s/sample for the four repeat measurements that constitute a single analysis (n=1 in Table 2). We use the 2s.e. of these four measurement as an assessment of our 'internal' error, reported with individual

analyses. Repeat analyses listed in Tables 1 and 2 involved separate dissolutions and chemical purifications, and should not be confused with repeats measured during a single analytical session. Based on the analysis of several international rock standards (Table 2), the $2\sigma_{SD}$ external reproducibility of the analyses is ±0.06‰ on $\delta^{26}Mg$.

Three separate methods of sample introduction were trialled for Mg isotope analysis. Firstly an Aridus (Cetac Instruments) desolvating nebuliser was used. Due to interferences, primarily CN^+ on ^{26}Mg, it is necessary to run the mass spectrometer in medium resolution ($M/\Delta M \sim 6000$, 5-95% peak edge width), resulting in the sensitivity being reduced by a factor of ~4-5 relative to standard 'low' resolution operation. The CN^+ interference is present even if the N_2 sweep gas to the Aridus is disconnected.

Secondly, we used a combination Scott double-pass cyclonic quartz spray chamber as in the study of Pogge von Strandmann, 2008. The problematic molecular, spectral interferences using the desolvating introduction system are largely absent under these wet plasma conditions. The C_2^+ and CN^+ intensities are less than 5000 ion counts per second (cps) at medium resolution and furthermore, there is no significant hydride formation ($MgH/Mg<10^{-6}$). Measurements are, therefore, made at low resolution, with no loss of sensitivity compared to desolvation at medium resolution. Approximately 50% of the samples presented here were analysed using the quartz spray chamber/low resolution method. This sensitivity is ~120pA of $^{24}Mg^+$ for a 200ng/ml solution at an uptake rate of 50µl/min. Background, instrumental Mg intensities, typically ~0.08pA ^{24}Mg, are subtracted from the sample intensities ^{24}Mg. Finally, an ApexQ (Elemental Scientific Inc.) introduction system was tested. This "moist" plasma introduction system allows for greater sensitivity (~100pA of $^{24}Mg^+$ for a 50ng/ml solution at an uptake rate of 50µl/min) than the quartz spray chamber setup described above, but is sufficiently free of spectral interferences to allow analysis at low resolution (CN^+ ~2000cps at medium resolution). All mineral separates and repeats of whole rocks were analysed by this method.

The results of the standards analysed by all three methods are identical within uncertainty and are presented in Table 2. The concordance of measurements made using three different introduction methods (Fig. 3) gives confidence in the accuracy of our procedures, because the introduction systems are likely differently sensitive to the presence of matrix and possibly influenced by different interferences (e.g. Teng et al.,

2010). In general, no systematic differences were observed in the internal or external uncertainty of measurements made using these different introduction systems.

The excellent mass bias stability and internal precision achievable on the Neptune allowed us to identify some important external influences on instrumental mass bias. Notably the mass flow controllers (especially the one regulating sample gas) responded to changes in air temperature of ≤2°C (during the cycles of the air conditioning system), causing resolvable periodic isotope ratio variations of ~0.1‰ on Mg isotope ratios. It is possible that such processes could affect analyses in other laboratories. To remove these artefacts, all Neptune mass flow controllers were subsequently water-cooled to our own design.

4.0 Results

4.1 Chondrite analyses

Bulk Li isotope compositions of chondrites show significant variability, although the range is less than for published data (Fig. 4a). Excluding finds (which may be weathered, and therefore have altered isotope ratios), enstatite chondrites have lighter Li isotopic compositions (δ^7Li = 1.7 ± 1.6‰ (2sd), n=7), than carbonaceous chondrites (3.3 ± 1.4‰, n=10) and ordinary chondrites (2.8 ± 1.5‰, n=11) (Table 1). Eucrites have similar δ^7Li to carbonaceous chondrites (3.3 ± 0.9‰, n=3), but our single aubrite has a very low δ^7Li of -0.3‰. Our δ^7Li values generally agree well with previously published data (James and Palmer, 2000; McDonough et al., 2003; Sephton et al., 2004; Sephton et al., 2006; Seitz et al., 2007). Interestingly, analyses of different chips of the same meteorite result in resolvable isotopic differences of up to 1.5‰. There are also similar isotopic differences compared to the data set of Seitz et al., 2007.

Bulk chondrite δ^{26}Mg values range from -0.38 to -0.15‰ (Table 1), with an average of -0.27‰. There is no difference in δ^{26}Mg between carbonaceous chondrites (average δ^{26}Mg = -0.29 ± 0.16‰ (2sd)), ordinary chondrites (average δ^{26}Mg = -0.28 ± 0.13‰) or enstatite chondrites (average δ^{26}Mg = -0.26 ± 0.08‰) (Fig. 4b). The δ^{26}Mg results from individual meteorites generally agree well with whole-rock results from most other studies (Galy et al., 2000; Baker et al., 2005; Teng et al., 2007; Wiechert and Halliday, 2007; Teng et al., 2010), but are resolvably heavier than the results from Chakrabarti and Jacobsen (2010).

All whole-rock chondrites measured plot within ±0.01‰ Δ^{25}Mg of the terrestrial fractionation line, in keeping with other studies (Bizzarro et al., 2004; Young and Galy, 2004; Baker et al., 2005; Teng et al., 2010). To provide more precise constraints on any possible mass-independent component, we have also recast our data into δ^{26}Mg* by mass fractionation correction of ^{26}Mg/^{24}Mg in all samples and standards to constant ^{25}Mg/^{24}Mg = 0.12663 (Catanzaro et al., 1966) and further "external" normalisation of samples to bracketing standards (Table 1). These chondritic mass independent Mg isotope ratios, average δ^{26}Mg* = 0.0029 ± 0.017‰, are indistinguishable from our terrestrial values, average = 0.0044 ± 0.022‰ (Thrane et al., 2008). We note, however, that our measurements were set up to determine precise mass dependent fractionation, which requires minimised time between bracketing standards, whereas for precise mass independent fractionation longer analysis times are needed e.g. (Schiller et al., 2010).

4.2 Whole-rock analyses

The results from the whole-rock peridotite analyses are shown in Table 1. Li concentrations in the ultra-mafic xenoliths vary between 0.5 and 4.8 μg/g, where the highest concentrations are in the Tok wehrlites. This is a similar concentration range to previously reported bulk peridotites (Brooker et al., 2004; Seitz et al., 2004; Magna et al., 2006b; Jeffcoate et al., 2007; Magna et al., 2008; Aulbach and Rudnick, 2009), but greatly exceeds the uncertainty on the estimate of the primitive mantle [Li] = 1.6 ± 0.5 μg/g (McDonough and Sun, 1995) or the variability in bulk carbonaceous and ordinary chondrites (1.3 ± 0.6 μg/g; Section 4.1).

Li isotope ratios in samples analysed in this study, -3.9 to +8.1‰ (average = 2.6‰, Fig. 5), show a similar range to previously determined bulk peridotites (Brooker et al., 2004; Seitz et al., 2004; Magna et al., 2006b; Jeffcoate et al., 2007; Magna et al., 2008; Aulbach and Rudnick, 2009). There is no clear overall trend between [Li] and δ^7Li, although the Avacha arc-peridotites generally show a positive trend of [Li] and δ^7Li, but over a much more limited range of [Li].

Mg isotope ratios of the peridotites vary between -0.35 and +0.06‰ (δ^{26}Mg), with an average of -0.21‰. There are no obvious trends between δ^{26}Mg and the considerable range of Mg# (or MgO), although in general isotopically lightest

366 samples have the highest Mg# (Fig. 5). It is worth noting that the full range in $\delta^{26}Mg$
367 is much smaller relative to reproducibility (±0.06‰, 2sd) than for $\delta^{7}Li$ (±0.3‰).
368
369 *4.3 Mineral separates*
370 The Li and Mg isotope compositions of mineral separates from several
371 peridotites were also determined (Table 3). Three samples from Tok, for which we
372 have measured whole-rock Li isotope compositions, have also had olivine and
373 clinopyroxene separates analysed for $\delta^{7}Li$ by Rudnick and Ionov (2007). These Tok
374 peridotites show clear evidence of Li isotope modification by diffusion, demonstrated
375 by the very low $\delta^{7}Li$ in clinopyroxene relative to olivine (Rudnick and Ionov, 2007).
376 The Avacha xenoliths, on the other hand, exhibit very little variation in inter-mineral
377 $\delta^{7}Li$ (Fig. 6; Table 3). Some separates from Avacha have previously been analysed by
378 Ionov and Seitz (2008) and compare well to our [Li] and $\delta^{7}Li$ values, given the larger
379 uncertainties of the previous study. The Avacha data from this study are also within
380 the range in isotope ratio and concentration measured for different Avacha samples by
381 Halama et al., 2009.
382 Mg isotope compositions were analysed in minerals of two Tok lherzolite-
383 wehrlite series peridotites, a Tok lherzolite-harzburgite series peridotite, an Avacha
384 sample, a phlogopite-bearing spinel lherzolite (4230-16) and two samples which best
385 represent unaltered peridotite (Mo-101 and 314-56), where the latter samples have
386 been shown to have $\delta^{7}Li$ values in cpx which are higher or similar compared to
387 coexisting olivine (Jeffcoate et al., 2007). This is significant, as it appears that kinetic
388 processes during xenolith entrainment and eruption cause the $\delta^{7}Li$ in clinopyroxenes
389 to become lighter than co-existing olivines (Jeffcoate et al., 2007; Rudnick and Ionov,
390 2007). For all samples, the Mg in clinopyroxene was found to be isotopically heavier
391 than coexisting olivine (Fig. 6), which is in agreement with the results from other
392 studies (Young et al., 2002; Wiechert and Halliday, 2007; Handler et al., 2009; Yang
393 et al., 2009; Young et al., 2009; Chakrabarti and Jacobsen, 2010). Coexisting olivine
394 and orthopyroxene were isotopically irresolvable in their $\delta^{26}Mg$ (Table 3).
395
396 5.0 Discussion
397 *5.1 Comparison to published standard data*

Several international rock standards were analysed for Li and Mg isotopes that span a range of relevant matrices for this and future studies of mantle derived samples: JP-1 (peridotite), BHVO-2 (ocean island basalt), BCR-2 (flood basalt) and JB-2 (arc basalt). For Mg isotope measurements, most of these rock standards were processed using both HCl and HNO_3 separation procedures (see methods), and yielded identical results within analytical uncertainty (Table 2; Fig. 3). In addition, the pure Mg solution standard CAM-1 and the normalising standard DSM-3 were passed through chemistry to ensure that the separation procedure does not induce artefacts (Table 2). Seawater and carbonate values, processed by the same methods, are reported elsewhere (Pogge von Strandmann, 2008; Foster et al., 2010).

The results from CAM-1 and rock standards analysed using desolvation nebulisation (Aridus and medium resolution), a quartz spray chamber and an Apex introduction system are identical (Fig. 3), as too are results using both HNO_3- and HCl-based chemistries.

The measured value of the standard JP-1 ($\delta^{25}Mg$ = -0.13 ± 0.04‰; $\delta^{26}Mg$ = -0.25 ± 0.05‰; 2sd, n=41, 29 dissolutions) differs considerably from the value reported by Wiechert and Halliday (2007) of +0.03‰ on $\delta^{25}Mg$ ($\delta^{26}Mg$ for JP-1 was not reported by these authors). This disparity has led us to conduct a standard addition experiment. In this we mixed JP-1 with CAM-1, without adding additional matrix (Tipper et al., 2008). Our three point determination (Fig. 7) is sufficiently precise to support our lighter value for JP-1, in contrast with Wiechert and Halliday (2007), but in keeping with Handler et al., 2009 ($\delta^{26}Mg$ = -0.23 ± 0.07‰).

Checking values of sample and standard by the standard addition approach usefully guards against some but not all sources of inaccuracy. This method does not isolate the influence of artefacts that are proportional to the mass of sample in the mix, such as isobaric interferences or mass bias influences that are linearly related to sample impurity. We feel our concordant results using several different chemistries and introduction systems, however, have already indicated that such concerns are not important in this study. We note, however, that the recent work of Chakrabarti et al., (2010) reports much lighter Mg isotope ratios in chondrites and peridotites than this or all other recent studies. Further work needs to be undertaken to account for this discrepancy.

Finally, two separate San Carlos olivines were analysed on the same xenolith studied by Jeffocate et al., 2007, with an average δ^{26}Mg of -0.30‰ (-0.34 to -0.27‰). Previous analyses of San Carlos olivines have shown a wide range of δ^{26}Mg (-0.68‰ (Teng et al., 2007), -0.06‰ (Wiechert and Halliday, 2007), -0.17‰ (Handler et al., 2009), -0.55‰ (Chakrabarti and Jacobsen, 2010), -0.25‰ (Young et al., 2009) and -0.27‰ (Liu et al., 2010). However, there is a significant compositional range in San Carlos peridotites (Frey and Prinz, 1978; Galer and O'Nions, 1998) and published Mg isotope analyses have not been made on the standardised Smithsonian Museum San Carlos olivine (USNM 111312/444). Moreover, Jeffcoate et al. (2007) documented extreme, kinetically induced, Li isotopic heterogeneity in their San Carlos sample. Thus it is unclear whether this variation in reported Mg isotope compositions of San Carlos olivines is due to sample heterogeneity or inaccuracies in isotope analysis. Nevertheless, this problem cannot pertain to the differences in the studies of Young et al., 2009 and Liu et al., 2010 compared to Chakrabarti and Jacobsen (2010), as all groups measured splits of the same powdered San Carlos olivines.

5.2. Chondrite analyses

In order to investigate the influences of terrestrial processes on the isotope ratios of the mantle, its initial composition must be established. One method to gauge the composition of the primitive mantle is to study chondritic material e.g. (Palme and O'Neill, 2003). Carbonaceous and ordinary chondrites have Li isotope compositions which are similar both to each other and to other studies' inferred bulk isotopic compositions of the mantle (Brooker et al., 2004; Magna et al., 2006b; Jeffcoate et al., 2007). Although there is variability in δ^{7}Li beyond analytical error, there is no clear relationship of isotope ratio with petrographic grade or meteorite group (Table 1, Fig. 4). An average of these analyses may provide a reasonable estimate of primitive mantle (3.1±1.3‰).

Our averaged analyses of enstatite chondrites have significantly lower δ^{7}Li than ordinary and carbonaceous chondrites (Fig. 4). Similarly, our one enstatite achondrite (aubrite) also has a very low δ^{7}Li value. Enstatite chondrites and enstatite achondrites are thought to have the same or similar parent bodies, given that they have identical oxygen isotope ratios (Clayton et al., 1984), and partial melting of an enstatite chondrite yields aubritic material (McCoy et al., 1999). Our observations are

463 somewhat different to those of Seitz et al. (2007), who reported the lowest meteoritic
464 δ^7Li for H4 and H5 ordinary chondrites, although both studies report identical δ^7Li for
465 the only duplicated enstatite chondrite (Indarch). It is possible that the small sample
466 sizes analysed from significantly heterogeneous meteorites (Sephton et al., 2004 and
467 below) have biased the results of ourselves and others.
468 Whilst the variability in δ^7Li ~1.5‰ between different sub-samples of the
469 same meteorite can account for scatter within each chondrite group, the difference of
470 ~1.5‰ between the mean of enstatite and other chondrites suggests a more systematic
471 process at work. The production of Li by low-energy spallation reactions in the early
472 solar system (Feigelson et al., 2002) should produce material which is isotopically
473 light with δ^7Li of ~-850‰ (Chaussidon et al., 2001). A spallogenic component has
474 been indetified in the refractory inclusions of several meteorites (Chaussidon and
475 Robert, 1998; Chaussidon et al., 2001). It has long been suggested that the reduced
476 nature of the parent bodies of enstatite chondrites implies they formed closer to the
477 sun than the other chondrites or achondrites (Kallemeyn and Wasson, 1986) and thus
478 are comprised of material most strongly influenced by early, solar spallation. In
479 addition, these isotopically light enstatite chondrites and the aubrite tend to have
480 higher ^{21}Ne/^{22}Ne than the other chondrites measured here, suggesting a greater
481 component of spallogenic ^{21}Ne (Schultz and Franke, 2004). Although the depth of
482 penetration for spallogenic production of ^{6}Li vs. ^{21}Ne is very different, both processes
483 likely occurred before larger parent bodies formed.
484 It is worthwhile considering our bulk analyses in the context of the discovery
485 of δ^7Li variations of >15‰ in different constituents of Murchison (CM2): -1.9‰ in
486 chondrules, but δ^7Li ~ +6‰ in phyllosilicate-rich matrix, and values >+13‰ in
487 carbonate-rich phases (Sephton et al., 2004). Such variability is supported by our
488 analysis of Allende chondrules (-0.3‰), which is significantly lighter than the bulk
489 meteorite (+2.7‰). Such variations have been interpreted as the result of aqueous
490 alteration, and the subsequent formation of phyllosilicates, driving bulk chondrites to
491 heavier values (James and Palmer, 2000; McDonough et al., 2003; Sephton et al.,
492 2004). It is not clear, however, why aqueous alteration should drive bulk
493 carbonaceous chondrites to similar values with no obvious trend of increasing δ^7Li
494 with increasing amount of aqueous alteration, i.e. from anhydrous CV/CO through
495 CM to CI. Although our analysis of Orgeuil (CI) is marginally isotopically heavier

than the other chondrites, Murchison (CM) is no heavier than Kainsaz (CO). The role of spallation in making chondrules isotopically light in Li is an intriguing possibility, but requires further investigation. Regardless of the cause of the heterogeneity, it is clear that measuring small fragments of chondrite may result in irreproducible δ^7Li values, as shown by our variable δ^7Li from different sub-samples of Orgueil, Murchison and Parnallee. That precise measurements could be made on such small sample sizes (Table 1) guided our approach in this study but further work on larger samples is required to provide a more definitive meteoritic reference.

In contrast to Li isotopes, the bulk Mg isotope compositions of the analysed chondrite groups are uniform, and within analytical uncertainty of the average (average δ^{26}Mg = -0.27 ± 0.12‰ (2sd)).

5.3 Establishing isotope compositions of the fertile mantle

5.3.1 Li isotopes in the fertile mantle

A number of xenoliths (Mo-101, 314-56, 313-102, 314-58) were selected on the basis of their major element composition as representative of fertile peridotites, namely a composition that can readily melt to produce basalt (i.e. MgO < 40 wt%, CaO and Al_2O_3 > 3 wt%, FeO ~ 8 wt% and Mg# ~ 0.89 (Ringwood, 1975; Sun, 1982; McDonough, 1990; Ionov, 2007); Fig. 1). That clinopyroxenes have higher or similar δ^7Li to associated olivines in some of these samples (314-58, 313-102, 314-56 (Magna et al., 2006a; Jeffcoate et al., 2007)) has been used to infer the absence of a late-diffusive influence on their δ^7Li (Jeffcoate et al., 2007). These fertile samples have an average Li concentration of 1.6 ± 0.7 μg/g, and an average δ^7Li of 3.2 ± 1.2‰. This range agrees well with that measured for carbonaceous chondrites and ordinary chondrites by this study (δ^7Li = 3.3 ± 1.4‰ and 2.8 ± 1.5‰, respectively; Section 5.2). We thus concur with Jeffcoate et al. that δ^7Li ~3.5‰ is a reasonable value for the "pristine" upper mantle.

For two of these xenoliths there are published whole rock δ^7Li analyses (reconstituted from mineral separates (Jeffcoate et al., 2007)) that agree with our bulk rock analyses; one (314-56) is a spinel lherzolite, the other (313-102) is a garnet lherzolite (Jeffcoate et al., 2007), and give δ^7Li = 3.5 ± 0.5‰. In contrast the bulk rock δ^7Li of 314-58 calculated from individual mineral analyses (Magna et al., 2006a)

528 differ from our bulk rock by ~1.4‰. This may be due to xenolith-scale heterogeneity,
529 which is discussed below.
530
531 5.3.2 Mg isotopes in the fertile mantle
532 Our equilibrated, fertile samples (detailed in Section 5.3.1) have an average
533 Mg# of 0.888 and an average δ^{26}Mg of -0.21 ± 0.07‰ (Fig. 5), which we propose as a
534 value for the upper mantle. This δ^{26}Mg is slightly higher but overlaps within
535 uncertainty the value for bulk chondrites (-0.27 ± 0.12‰; Section 5.2). Statistical
536 analysis (student-t) shows that the populations of fertile peridotite and carbonaceous
537 chondrites are distinct at the 95% confidence level. However this test assumes that
538 each population represents a single base value, which may not be the case, due to
539 diffusive alteration and/or equilibrium fractionation between minerals (see below). As
540 discussed above, our bulk mantle value is also within analytical uncertainty of the
541 values recently suggested by five other comprehensive studies (Handler et al., 2009;
542 Yang et al., 2009; Young et al., 2009; Bourdon et al., 2010; Teng et al., 2010), and we
543 suggest that this value is now rather well constrained: primitive mantle olivines of
544 Handler et al. (2009) average -0.27 ± 0.14‰, those of Young et al. (2009) average -
545 0.25 ± 0.16‰, whilst bulk rock averages -0.26 ± 0.16‰, -0.25 ± 0.07 and -0.22 ±
546 0.04‰ are reported by Yang et al. (2009), Teng et al. (2010) and Bourdon et al.
547 (2010), respectively.
548
549 *5.4 Mg and Li isotope covariation*
550 One of the more striking results of this study is the wide range in bulk xenolith
551 δ^{7}Li and δ^{26}Mg (Fig. 8). This variability is significantly in excess of that seen in the
552 chondrites or inferred fertile mantle samples (Sections 5.3; Fig. 4 & 5). In terms of
553 δ^{26}Mg, this spread is greater than that reported by Teng et al., 2010 (0.07‰), but
554 similar to that reported by Yang et al., 2009 (0.34‰). This variability in Mg and Li
555 isotope compositions allows the xenoliths to be divided into three groups: 1) five
556 samples with negative δ^{7}Li and generally the lowest Mg isotope ratios; 2) the bulk of
557 samples with δ^{7}Li extending from 1.2 to 5.9‰ and δ^{26}Mg from -0.29 to -0.06‰; 3) a
558 single wehrlite, which has both very high δ^{7}Li and δ^{26}Mg. Overall there appears to be
559 a positive co-variation between δ^{7}Li and δ^{26}Mg in these samples.

A number of processes are potential candidates for perturbing the Li and Mg stable isotope ratios of these xenolith samples, such as melt depletion, metasomatism, in particular of the type that caused the wehrlitisation of several samples (Ionov et al., 2005b), equilibrium fractionation and diffusion (kinetic fractionation). Samples from Tok, Tariat and Avacha have also been analysed for Fe isotope variations (Weyer and Ionov, 2007). Only three of those samples have distinct δ^{56}Fe from the normal mantle, probably caused by interaction of the residual peridotite with evolved, high [Fe] silicate melts (Weyer and Ionov, 2007). There is no correlation of δ^{7}Li or δ^{26}Mg with δ^{56}Fe, which shows that the Li and Mg systems remain unaffected by this metasomatism that lowered the Mg# of some samples. We will explore the other possibilities below.

5.4.1 Isotopically light xenoliths

Several studies have implicated the role of diffusion in creating strikingly isotopically light Li in clinopyroxenes as a result of incomplete re-equilibration of xenoliths with host basalt in response to changing conditions during ascent or post-eruptive cooling (Jeffcoate et al., 2007; Rudnick and Ionov, 2007; Tang et al., 2007; Ionov and Seitz, 2008; Kaliwoda et al., 2008; Aulbach and Rudnick, 2009). Likewise we infer that diffusive processes have resulted in the low δ^{7}Li seen in some bulk xenoliths in this study. That δ^{26}Mg is low in the same samples with low δ^{7}Li suggests that Mg is also affected by diffusive processes. As with all stable isotopes, the lighter isotope, ^{24}Mg, diffuses faster than the heavier isotopes, and this process has been demonstrated in melting experiments, by both chemical diffusion (Richter et al., 2008) and Soret diffusion (Huang et al., 2010a), in komatiite olivines (Dauphas et al., 2010) and in evaporation of forsterite (Wang et al., 1999; Yamada et al., 2006). Further, elemental Mg has long been known to diffuse on the crystal scale, and also over longer (cm-m) distances via grain boundary diffusion e.g. (Sanford, 1982; Miller et al., 2009).

This mechanism of net diffusion of Li and Mg from host melt into xenolith contrasts with the closed system model of Ionov and Seitz (2008), who accounted for the isotopically light cpx in slowly cooled xenoliths as a result of inter-grain redistribution of Li between olivine and cpx. This process may also occur, but our

592 bulk isotope measurements clearly demonstrate that the xenoliths in question must
593 have behaved as open systems with respect to Li and Mg.
594
595 *5.5 Modelling the isotopic covariation*
596 If the trend towards light Li and Mg isotopes described above is due to
597 diffusion, it should be possible to model the relative behaviours of the two systems.
598 High temperature diffusion and corresponding kinetic isotope fractionation
599 dominantly depends on three variables: 1) the diffusivity (diffusion coefficients) D of
600 the element; 2) the concentration gradients, or more correctly the chemical potential
601 gradients between phases; 3) the kinetic isotope fractionation parameter (β) (Richter
602 et al., 1999). The isotopic diffusivities and β are related by the expression $D_2/D_1 =$
603 $(m_1/m_2)^{\beta}$, where D_1 and D_2 are the diffusivities of isotopes with the masses m_1 and m_2
604 (Richter et al., 2003).
605 From a mass balance point of view, it would be hard to alter the Mg budget of
606 the bulk mantle by diffusive interaction with a relatively small volume melt or fluid.
607 This suggests that diffusive alteration of Mg can occur solely after xenolith removal
608 from its source. Although the xenolith has a much higher Mg content than the melt,
609 the small volume of the xenolith relative to the entraining flow means there is still
610 sufficient Mg to affect its bulk composition.
611 Li diffusion may result from the high incompatible element contents of the
612 entraining melts, such that their Li concentrations exceed those in equilibrium with
613 the typically melt-depleted mantle xenoliths (Jeffcoate et al., 2007). Further, an
614 increase in the partition coefficient of Li during lava cooling may also lead to
615 diffusion of Li from the melt into the xenolith (Jeffcoate et al., 2007; Gallagher and
616 Elliott, 2009). The driving force of Mg isotope fractionation is less clear, as the
617 peridotites frequently have higher Mg# than would be anticipated for equilibrium with
618 their host basalts. We tentatively suggest that Mg diffusion is driven by the need to
619 charge balance during the dehydration of nominally anhydrous minerals (Bell et al.,
620 2004; Kohn and Grant, 2006), as they approach the surface and degas. Our
621 observations appear to implicate Mg diffusion into the xenoliths, which is consistent
622 with this hypothetical mechanism.
623 The basic scenario envisaged for the model assumes that small spherical
624 xenoliths, with a starting composition equal to the fertile mantle, interact with large

(effectively infinite) volumes of melt (Crank, 1975). Rather than assuming that each xenolith is a solid sphere (which would result in only the xenolith boundaries becoming affected by diffusion), we assume that fast transport occurs along all the xenolith grain boundaries (Dohmen et al., 2010), followed by diffusion into individual crystals. The model integrates the crystal data to acquire a whole-rock xenolith isotope ratio, which initially becomes isotopically lighter as Li and Mg diffuse in, and eventually returns to an equilibrium value with time (Fig. 9, shown for crystal diameters of 1mm). The relative distance the isotopic anomalies of Li and Mg can diffuse in a given time is determined by the relative diffusivities D_{Mg}/D_{Li}, and this parameter is therefore key. In contrast, the relative chemical potential gradients and β control the depths of the troughs. The model uses chemical gradients and β values that best-fit our data, and are similar to those established experimentally (Richter et al., 2003; Richter et al., 2008; Richter et al., 2009) (Fig. 10).

In theory diffusive influx of Mg should result in olivine rims with elevated Mg concentrations. One of the light samples, Tok 6-3, was analysed with an electron micro-probe. No MgO gradient could be resolved, with the uncertainty of ±0.4 wt%. This gives an upper limit for diffusional modelling: given our proposed β of ~0.1-0.15 (see below), to perturb a 2mm diameter olivine from a primitive starting composition to the composition measured now, the perturbed rim would require a width of 3-5μm. In addition, even if the MgO gradient were larger, the resolution of the electron micro-probe would not be sufficient to resolve the rim.

Figure 10 shows the results of the modelled co-diffusion of Li and Mg. Each line of constant D_{Mg}/D_{Li} represents the evolving xenolith composition with the arrows indicating direction of increasing time: the isotopic trough of the faster diffusing element (Li, except when $D_{Mg}/D_{Li} = 1$) arrives first, driving the path to lighter values along the y-axis (δ^7Li). Following this, the second trough (that of Mg) arrives, driving the path to lighter x-axis (δ^{26}Mg) values. Bearing in mind the analytical uncertainty on the data, the isotopically lightest values appear to be best modelled by setting $D_{Mg}/D_{Li} = 0.25\text{-}1$, implying Mg diffusivity that is within an order of magnitude of that of Li. The relative diffusivities during Li tracer diffusion and Mg interdiffusion have been experimentally shown to vary by several orders of magnitude, depending on the host material. Thus in basaltic melts D_{Mg}/D_{Li} ~0.01 (Richter et al., 2003), but in olivine the relative diffusivities are thought to be within an order of magnitude

658 (D_{Mg}/D_{Li} ~0.1) (Dohmen et al., 2010), a factor of 3 (D_{Mg}/D_{Li} ~0.3) (Qian et al., 2010)
659 or even less than a factor of 1-2 (D_{Mg}/D_{Li} ~0.6-1.15, depending on crystallographic
660 axis) (Spandler and O'Neill, 2010), i.e. well within the bounds required by our model.
661 This behaviour has been explained by suggesting that element diffusivity in olivine is
662 controlled by cation site preference, charge balance mechanisms and point-defect
663 concentrations (Spandler and O'Neill, 2010).
664 Given that olivine is the major host of both Li (Seitz and Woodland, 2000) and
665 Mg in the mantle, diffusion in olivine would be expected to be the rate-limiting step to
666 evolving bulk xenolith Mg and Li isotope composition. Since the diffusivities of Li
667 and Mg in olivine are sufficiently well known (Dohmen et al., 2010), our model can
668 predict the time required for the isotopic perturbations to occur (i.e. the time elapsed
669 between removal of the xenolith from the wall-rock, and attainment of the closure
670 temperature for diffusion; Fig. 9). The model is simplified, because it does not factor
671 in decreasing diffusivity with cooling, but rather assumes that the initial temperature
672 is maintained until closure occurred. As such the model can only provide minimum
673 estimates of diffusion duration. As shown in Fig. 9, attainment of lowest δ^{7}Li and
674 δ^{26}Mg values is relatively rapid (~5-10 years), whereas re-equilibration occurs over
675 much longer timescales (>30 years). This suggests that the isotopically lightest
676 samples were entrained and experienced diffusive ingress of Li and Mg for ~10 years.
677 This timescale is approximately an order of magnitude greater than cooling of even
678 thick basaltic lava flows. Calculations suggest that for a cooling period of 10 years, a
679 flow ~50m thick would be required, whereas in reality basaltic flows are rarely more
680 than ~5m thick, and cool on the order of weeks (Flynn et al., 1994). This strongly
681 suggests that the diffusive perturbation was imparted to the xenoliths during processes
682 that occurred prior to eruption, but post removal of the xenolith from the wall rock.
683 Assuming the model parameters are correct, this would imply that the
684 xenolith transit time for these isotopically light samples was on the order of 10 years,
685 and suggests storage of the xenoliths for a period of years between entrainment and
686 final cooling. The small role played by post-eruptive cooling rate seems at odds with
687 the empirical relationship observed by Ionov and Seitz, 2008 for diffusive
688 perturbation of xenoliths depending on their mode of eruption, i.e. in rapidly cooled
689 pyroclastic deposits or slowly cooled flows. We instead suggest that the key timescale
690 is that between host-magma degassing, which we infer to drive Mg diffusion, and

691 eruption. The H^+ content of kimberlitic xenoliths is more than sufficient for its
692 replacement by Mg to perturb the bulk xenolith $\delta^{26}Mg$ by ~0.2‰ (Bell et al., 2004;
693 Grant et al., 2006; Kohn and Grant, 2006; Grant et al., 2007). A magma degassed
694 years before eruption should have diffusionally perturbed xenoliths but is likely to
695 erupt as a flow. In contrast, undegassed magmas are likely to erupt explosively and
696 have more pristine xenoliths.
697
698 *5.6 Inter-mineral Mg isotope fractionation*
699 Young et al. (2009) calculated theoretical equilibrium Mg isotope
700 fractionation between pure forsterite and diopside, orthoenstatite and spinel. Forsterite
701 should be the isotopically lightest of these minerals, which is substantiated by results
702 from both this and other studies (Young et al., 2002; Wiechert and Halliday, 2007;
703 Handler et al., 2009; Young et al., 2009; Chakrabarti and Jacobsen, 2010). Theoretical
704 equilibrium values predict a forsterite-diopside $\Delta^{26}Mg$ ~ 0.08-0.1‰ in the temperature
705 range 850-1000°C. Measured values range from 0.04-0.31‰ (this study; Fig. 6),
706 <0.24‰ (Handler et al., 2009), <0.23‰ (Chakrabarti and Jacobsen, 2010), 0.11-
707 0.14‰ (Wiechert and Halliday, 2007). This variation may be due to varying
708 mineralogy, or kinetic effects on top of any equilibrium fractionation.
709 The anomalously heavy $\delta^{26}Mg$ of wehrlite, Tok 10-1 is readily related to its
710 high modal abundance of isotopically heavy cpx (Table 3). This sample has seen
711 complete replacement of opx by cpx (Ionov et al., 2005b). It also shows the greatest
712 $\Delta^{26}Mg_{cpx\text{-}ol}$ which may indicate a non-equilibrium component in this fractionation
713 factor (Fig. 6). During pyroxene replacement, Mg from opx will be diffusively lost to
714 the melt, and replaced by Ca, potentially driving the $\delta^{26}Mg$ of the residual pyroxene
715 isotopically heavy (this process also explains why there is no overriding correlation
716 for our samples between isotope ratios and mineral ratios such as cpx/ol). This sample
717 also has high [Li], suggesting that the infiltrating melt that caused wehrlitisation was
718 Li-rich. The high δ^7Li of Tok 10-1 could therefore just reflect the isotopic
719 composition of this interacting melt. Alternatively, given the high [Li] of the
720 wehrlitised mantle, the concentration gradient thus established with the surrounding
721 mantle resulted in subsequent diffusive loss of Li and an increase in the δ^7Li of the
722 residue. This suggests that the relatively high $\delta^{26}Mg$ and δ^7Li of this sample may be

723 unrelated in mechanism, although both may ultimately have been caused by
724 metasomatic wehrlitisation.
725 In general, the wehrlite sample group shows high variability in both δ^{7}Li and
726 δ^{26}Mg. This is in agreement with Yang et al. (2009), who reported δ^{26}Mg variability
727 of 0.34‰ in wehrlites from the North China craton. However, Yang et al. (2009)
728 reported low δ^{26}Mg values for some wehrlites (down to -0.44‰). Taken together with
729 results from this study, this may suggest that the isotope composition of wehrlites are
730 strongly dependent on the composition of the wehrlitising agent, and the mechanism
731 of mineral replacement that occurs during these reactions.
732 If pyroxenes in equilibrium with olivine are ~0.06-0.08 (δ^{26}Mg, opx) and
733 0.09-0.13‰ (cpx) (Young et al., 2009) heavier, then it would be expected that fertile
734 mantle peridotites are ~0.03‰ heavier than analyses of their constituent olivines.
735 This could account for a degree of the minor offset between our data for bulk samples
736 and those of Handler et al. (2009) for olivines, but such small differences are difficult
737 to discern.
738
739 *5.7 Arc peridotites*
740 The Avacha peridotite xenoliths are thought to represent fragments of mantle
741 wedge lithosphere which sits above the subducting Pacific plate at the Kurile-
742 Kamchatka trench (Ionov and Seitz, 2008; Ionov, 2010), and as such probably have
743 been affected by percolation of metasomatic fluids which initially derive from the
744 dehydrating slab. These initial fluids are generally assumed to be concentrated in Li
745 (≤200 μg/g (Ryan and Langmuir, 1987; Marschall et al., 2007a)) and preferentially
746 enriched in ^{7}Li (Chan and Kastner, 2000; Tomascak et al., 2000; Tomascak et al.,
747 2002; Elliott et al., 2004), in theory causing the hydrated wedge to become more
748 concentrated in Li and isotopically heavier (Tomascak et al., 2002). In contrast, given
749 the low Mg content of the crust, and therefore the subducting slab, it is unlikely that
750 fluids from slab dehydration could resolvably affect the Mg budget of the mantle
751 wedge.
752 The δ^{7}Li of our arc peridotites ranges from 2.5 to 6.0‰, i.e. from a
753 composition slightly lighter than that of the primitive mantle to one which is much
754 heavier. The Avacha samples also show a significant co-variation between δ^{7}Li and
755 [Li] (r^2=0.66) as well as FeO (r^2=0.77; Fig. 11) and MnO (r^2=0.6), and are negatively

correlated with Mg#. The positive correlation of δ^7Li and [Li] with FeO argues against the hypothesis (Ionov 2010) that FeO and Mg# variations in the Avacha suite stem from differences in melting depth (FeO in residues decreases with depth), because there is no reason why δ^7Li and [Li] should be lower in deeper melting residues as well.

Mineral separate analysis of some of the Avacha samples (Table 3) show coexisting olivine, orthopyroxene and clinopyroxene to be in inferred elemental (Woodland et al., 2002) and isotopic (Jeffcoate et al 2007) equilibrium for Li. These data agree with other Li studies from Avacha (Ionov and Seitz, 2008; Halama et al., 2009). Inter-mineral δ^{26}Mg values are also within reproducibility of theoretical equilibrium fractionation (Young et al., 2009). This implies that the δ^7Li and δ^{26}Mg of these arc xenoliths have not been diffusively altered during transport to the surface but represent signals from deeper in the mantle.

Thus the correlated enrichments in δ^7Li, [Li], FeO and MnO are likely due to metasomatism by an isotopically heavy, Fe-rich, slab-derived fluid. In addition, there is a positive correlation between δ^{26}Mg and FeO (r^2=0.94, thus leading to the apparent co-variation between δ^7Li and δ^{26}Mg in Fig. 8), although individual samples are only just resolvable at the 2s.e. level. The xenoliths with high FeO will have experienced greater influx of Fe, and therefore interdiffusional removal of Mg, potentially driving xenolith δ^{26}Mg towards higher values. Ionov (2010) inferred that the Avacha peridotites may have been affected by melt metasomatism soon after their partial melting (i.e. in the asthenosphere), and also by fluid infiltration in the lithosphere shortly before their transport to the surface. The latter event produced minor amphibole and enrichments in incompatible trace elements, which are petrographically clear as veins (Halama et al., 2009; Ionov, 2010). The δ^7Li or [Li] show no correlation ($r^2 \leq 0.1$) with La, Sr, Ba or modal amphibole, although the sample with most amphibole does have high δ^7Li and δ^{26}Mg. Hence for the suite as a whole there is no control of the most recent event on δ^7Li. We conclude that the enrichment in δ^7Li and [Li] occurred in an older, asthenospheric event.

If the high δ^7Li signal in these arc peridotites stems from metasomatism in the asthenosphere, then this suggests that it represents an isotopically heavy mantle wedge caused by dehydration of the subducting slab. The dehydrated slab is thought to become isotopically lighter by δ^7Li ≤3‰ (Marschall et al., 2007b), whilst the slab-

789 derived fluids are isotopically heavy, in turn causing the hydrated mantle wedge to
790 also become isotopically heavy (Elliott et al., 2004). The Avacha xenoliths may
791 therefore demonstrate that the hydrated wedge is indeed enriched in ^{7}Li, and that this
792 fractionation can survive emplacement to the surface (at least in xenoliths erupted in
793 rapidly-cooled pyroclastic deposits). Given that the Avacha samples plot along a δ^{7}Li
794 vs. 1/[Li] mixing line, a simple mixing model (assuming that all samples interacted
795 with a fluid of the same composition) suggests that the fluid component had a δ^{7}Li ~
796 9‰.
797 Although diffusion may alter the bulk rock Li and Mg isotopic compositions
798 of slowly emplaced or cooled degassed xenoliths, more rapid processes, and
799 potentially a lack of degassing, appear to allow deep-mantle signatures to survive.
800 Trends towards isotopically heavy Li have been reported in MORB glasses, and were
801 interpreted as recycling of an isotopically heavy mantle component into the mid-
802 ocean ridges (Elliott et al., 2006). It is now clear that the metasomatised mantle wedge
803 is a plausible source of this isotopically heavy Li reservoir, which is viscously
804 coupled to the down-going slab, and so mixed into the convecting mantle.
805
806 6.0 Conclusions
807 This study has analysed Li and Mg isotopes in whole-rock chondrites and
808 peridotites from several global localities. Carbonaceous chondrites give: δ^{7}Li = 3.3 ±
809 1.4‰ (2sd), δ^{25}Mg = -0.15 ± 0.08‰ and δ^{26}Mg = -0.29 ± 0.16‰. Enstatite chondrites
810 have lower δ^{7}Li than carbonaceous chondrites by ~2‰, possibly implicating their
811 derivation from material that orbited closer to the early sun and underwent enhanced
812 spallation due to its irradiation. This interpretation must be treated with caution, given
813 the well-documented Li isotope heterogeneity in chondrites and needs to be tested
814 using analyses of larger sample sizes. Analyses of fertile xenoliths that exhibit no
815 evidence of diffusive perturbation of Li suggest that the composition of the bulk
816 primitive mantle is δ^{7}Li = 3.5 ± 0.5‰, δ^{25}Mg = -0.10 ± 0.04‰ and δ^{26}Mg = -0.21 ±
817 0.07‰, within error of carbonaceous and ordinary chondrites.
818 In contrast, the total measured range in xenolithic, continental bulk peridotites
819 with variable amounts of metasomatism and melt depletion is ~13‰ (δ^{7}Li) and
820 ~0.4‰ (δ^{26}Mg). These ranges are easily analytically resolvable, and extend well
821 beyond the possible values of chondrites or the fertile mantle. A co-variation between

822 δ^7Li and δ^{26}Mg suggest that both isotope systems may be affected by the same
823 process/processes. Diffusion is strongly implicated in generating the general trend
824 from the fertile mantle towards isotopically light ratios. This co-variation has been
825 modelled and the isotopically lightest samples suites require relative diffusivities of
826 D_{Mg}/D_{Li} ~0.25-1, in keeping with experimental studies that have determined D_{Mg}/D_{Li}
827 ~0.1-1 in olivine. These known diffusivities of Li and Mg in olivine allow calculation
828 of cooling times of the xenoliths of ~5-10 years for isotopically light samples,
829 approximately an order of magnitude longer than the cooling to closure temperature
830 for the basaltic lava flows in which these xenoliths were erupted. This suggests
831 diffusive perturbation occurs during period of storage post-entrainment, but pre-
832 eruption. In contrast, xenoliths erupted in pyroclastic deposits do not show
833 anomalously light δ^7Li and δ^{26}Mg. We speculate that degassing of magmas both
834 drives diffusion of Mg (and Li) into entrained xenoliths, to charge balance hydrogen
835 loss from the minerals, and also influences the subsequent eruptive style (explosive or
836 effusive).
837 In the pyroclastic-hosted Avacha arc peridotites, Li isotopes trend to heavier
838 values at greater Li, FeO and MnO concentrations. This suggests that the Li isotope
839 system in the Avacha suite may have been affected by ingress of slab-derived fluids
840 with high δ^7Li, thus providing the isotopic signal of the hydrated mantle wedge.
841 The range in [Li], [Mg], δ^7Li and δ^{26}Mg in our xenoliths, which have large
842 variations in melt extraction, metasomatism and emplacement histories, suggest that
843 small xenoliths may be altered by diffusive isotope fractionation when emplaced in
844 large volumes of melts. This makes it difficult to determine pertinent information on
845 light elements in the mantle from such xenoliths, and such data should be rather
846 obtained on large pyroclastic-hosted xenoliths.
847
848
849 Acknowledgments
850 Simon Kohn, Fred Witham and Ralf Dohmen are thanked for discussions on the
851 hydration of the mantle, on lava cooling and on diffusion, respectively. The Natural
852 History Museum is thanked for providing the chondrite samples. PPvS was supported
853 by NERC grant NER/C510983/1. Paul Tomascak, Fang-Zhen Teng and an

anonymous reviewer are thanked for their comments. Shichun Huang is thanked for careful editing.

Aulbach, S. and Rudnick, R. L., 2009. Origins of non-equilibrium lithium isotopic fractionation in xenolithic peridotite minerals: Examples from Tanzania. *Chemical Geology* **258**, 17-27.

Baker, J., Bizzarro, M., Wittig, N., Connelly, J., and Haack, H., 2005. Early planetesimal melting from an age of 4.5662 Gyr for differentiated meteorites. *Nature* **436**, 1127-1131.

Bell, D. R., Rossman, G. R., and Moore, R. O., 2004. Abundance and Partitioning of OH in a High-pressure Magmatic System: Megacrysts from the Monastery Kimberlite, South Africa. *Journal of Petrology* **45**, 1539-1564.

Bizzarro, M., Baker, J. A., and Haack, H., 2004. Mg isotope evidence for contemporaneous formation of chondrules and refractory inclusions. *Nature* **431**, 275-278.

Bizzarro, M., Paton, C., Larsen, K., Schiller, M., Trinquier, A., and Ulfbeck, D., 2011. High-precision Mg-isotope measurements of terrestrial and extraterrestrial material by HR-MC-ICPMS—implications for the relative and absolute Mg-isotope composition of the bulk silicate Earth *Journal of Analytical Atomic Spectrometry* **26**, 565-577.

Black, J. R., Yin, Q. Z., and Casey, W. H., 2006. An experimental study of magnesium-isotope fractionation in chlorophyll-a photosynthesis. *Geochimica Et Cosmochimica Acta* **70**, 4072-4079.

Bourdon, B., Tipper, E. T., Fitoussi, C., and Stracke, A., 2010. Chondritic Mg isotope composition of the Earth. *Geochimica Et Cosmochimica Acta* **74**, 5069-5083.

Brooker, R. A., James, R. H., and Blundy, J. D., 2004. Trace elements and Li isotope systematics in Zabargad peridotites: evidence of ancient subduction processes in the Red Sea mantle. *Chemical Geology (Lithium Isotope Geochemistry)* **212**, 179-204.

Catanzaro, E. J., Murphy, T. J., Garner, E. L., and Shields, W. R., 1966. Absolute isotopic abundance rataios and atomic weight of magnesium. *Journal of Research of the National Bureau of Standards Section A - Physics and Chemistry* **A70**, 453-&.

Chakrabarti, R. and Jacobsen, S. B., 2010. The isotopic composition of magnesium in the inner Solar System. *Earth and Planetary Science Letters* **293**, 349-358.

Chakraborty, S., Farver, J. R., Yund, R. A., and Rubie, D. C., 1994. Mg Tracer Diffusion in Synthetic Forsterite and San-Carlos Olivine as a Function of P, T and Fo2. *Physics and Chemistry of Minerals* **21**, 489-500.

Chan, L. H., Edmond, J. M., Thompson, G., and Gillis, K., 1992. Lithium Isotopic Composition of Submarine Basalts - Implications for the Lithium Cycle in the Oceans. *Earth and Planetary Science Letters* **108**, 151-160.

Chan, L. H. and Frey, F. A., 2003. Lithium isotope geochemistry of the Hawaiian plume: Results from the Hawaii Scientific Drilling Project and Koolau volcano. *Geochem. Geophys. Geosyst.* **4**.

Chan, L. H. and Kastner, M., 2000. Lithium isotopic compositions of pore fluids and sediments in the Costa Rica subduction zone: Implications for fluid processes and sediment contribution to the arc volcanoes. *Earth and Planetary Science Letters* **183**, 275-290.

Chan, L. H., Lassiter, J. C., Hauri, E. H., Hart, S. R., and Blusztajn, J., 2009. Lithium isotope systematics of lavas from the Cook–Austral Islands: Constraints on the origin of HIMU mantle. *Earth and Planetary Science Letters* **277**, 433-442.

Chang, V. T. C., Makishima, A., Belshaw, N. S., and O'Nions, R. K., 2003. Purification of Mg from low-Mg biogenic carbonates for isotope ratio

determination using multiple collector ICP-MS. *Journal of Analytical Atomic Spectrometry* **18**, 296-301.

Chaussidon, M. and Robert, F., 1998. 7Li/6Li and 11B/10B variations in chondrules from the Semarkona unequilibrated chondrite. *Earth and Planetary Science Letters* **164**, 577-589.

Chaussidon, M., Robert, F., K.D., M., and Krot, A. N., 2001. Lithium and boron isotopic compositions of refractory inclusions from primitive chondrites: a record of irradiation in the early solar system. *Lunar and Planetary Science Conference* **XXXII**, 1862.

Clayton, R. N., Mayeda, T. K., and Rubin, A. E., 1984. Oxygen isotopic compositions of enstatite chondrites and aubrites. *Journal of Geophysical Research* **89**, C245-C249.

Crank, J., 1975. *The Mathematics of Diffusion*. Oxford University Press.

Dauphas, N., Teng, F. Z., and Arndt, N. T., 2010. Magnesium and iron isotopes in 2.7 Ga Alexo komatiites: Mantle signatures, no evidence for Soret diffusion, and identification of diffusive transport in zoned olivine. *Geochimica Et Cosmochimica Acta* **74**, 3274-3291.

Dohmen, R., Kasemann, S. A., Coogan, L., and Chakraborty, S., 2010. Diffusion of Li in olivine. Part I: Experimental observations and a multi species diffusion model. *Geochimica Et Cosmochimica Acta* **74**, 274-292.

Elliott, T., Jeffcoate, A., and Bouman, C., 2004. The terrestrial Li isotope cycle: light-weight constraints on mantle convection. *Earth and Planetary Science Letters* **220**, 231-245.

Elliott, T., Thomas, A., Jeffcoate, A., and Niu, Y. L., 2006. Lithium isotope evidence for subduction-enriched mantle in the source of mid-ocean-ridge basalts. *Nature* **443**, 565-568.

Feigelson, E. D., Garmire, G. P., and Pravdo, S. H., 2002. Magnetic Flaring in the Pre-Main-Sequence Sun and Implications for the Early Solar System. *The Astrophysical Journal* **572**, doi: 10.1086/340340.

Flesch, G. D., Anderson, A.R., Svec, H.J., 1973. A secondary isotopic standard for 6Li/7Li determinations. *Int. J. Mass Spectrom. Ion Process.* **12**, 265-272.

Flynn, L. P., Mouginis-Mark, J., and Horton, K. A., 1994. Distribution of thermal areas on an active lava flow field: Landsat observations of Kilauea, Hawaii, July 1991. *Bulletin of Volcanology* **56**, 284-296.

Foster, G. L., Pogge von Strandmann, P. A. E., and Rae, J. W. B., 2010. Boron and magnesium isotopic composition of seawater. *Geochem. Geophys. Geosyst.* **11**, Q08015, doi:10.1029/2010GC003201.

Frey, F. A. and Prinz, M., 1978. Ultramafic inclusions from the San Carlos, Arizona: petrological and geochemcial data bearing on their petrogenesis. *Earth and Planetary Science Letters* **38**, 129-176.

Galer, S. J. G. and O'Nions, R. K., 1998. Chemical and isotopic studies of ultramafic inclusions from San Carlos volcanic field, Arizona: a bearning on their petrogenesis. *Journal of Petrology* **30**, 1033-1064.

Gallagher, K. and Elliott, T., 2009. Fractionation of lithium isotopes in magmatic systems as a natural consequence of cooling *Earth and Planetary Science Letters* **278**, 286-296.

Galy, A., Belshaw, N. S., Halicz, L., and O'Nions, R. K., 2001. High-precision measurement of magnesium isotopes by multiple-collector inductively coupled plasma mass spectrometry. *International Journal of Mass Spectrometry* **208**, 89-98.

Galy, A., Yoffe, O., Janney, P. E., Williams, R. W., Cloquet, C., Alard, O., Halicz, L., Wadhwa, M., Hutcheon, I. D., Ramon, E., and Carignan, J., 2003. Magnesium isotope heterogeneity of the isotopic standard SRM980 and new reference materials for magnesium-isotope-ratio measurements. *Journal of Analytical Atomic Spectrometry* **18**, 1352-1356.

Galy, A., Young, E. D., Ash, R. D., and O'Nions, R. K., 2000. The Formation of Chondrules at High Gas Pressures in the Solar Nebula. *Science* **290**, 1751-1753.

Gorbatov, A., Kostoglodov, V., Suarez, G., and Gordeev, E., 1997. Seismicity and structure of the Kamchatka subduction zone. *Journal of Geophysical Research* **102**, 17883-17989.

Grant, K. J., Kohn, S. C., and Brooker, R. A., 2006. Solubility and partitioning of water in synthetic forsterite and enstatite in the system MgO-SiO2-H2O +/- Al2O3. *Contributions to Mineralogy and Petrology* **151**, 651-664.

Grant, K. J., Kohn, S. C., and Brooker, R. A., 2007. The partitioning of water between olivine, orthopyroxene and melt synthesised in the system albite-forsterite-H2O. *Earth and Planetary Science Letters* **260**, 227-241.

Halama, R., Savov, I. P., Rudnick, R. L., and McDonough, W. F., 2009. Insights into Li and Li isotope cycling and sub-arc metasomatism from veined mantle xenoliths, Kamchatka. *Contributions to Mineralogy and Petrology* **158**, 197-222.

Handler, M. R., Baker, J. A., Schiller, M., Bennett, V. C., and Yaxley, G. M., 2009. Magnesium stable isotope composition of Earth's upper mantle. *Earth and Planetary Science Letters* **282**, 306-313.

Huang, F., Chakraborty, P., Lundstrom, C. C., Holmden, C., Glessner, J. J. G., Kieffer, S. W., and Lesher, C. E., 2010a. Isotope fractionation in silicate metls by thermal diffusion. *Nature* **464**, 396-400.

Huang, F., Glessner, J., Ianno, A., Lundstrom, C. C., and Zhang, Z., 2009a. Magnesium isotopic composition of igneous rock standards measured by MC-ICP-MS. *Chemical Geology* **268**, 15-23.

Huang, F., Lundstrom, C. C., Glessner, J., Ianno, A., Boudreau, A., Li, J., Ferre, E. C., Marshak, S., and DeFrates, J., 2009b. Chemical and isotopic fractionation of wet andesite in a temperature gradient: Experiments and models suggesting a new mechanism of magma differentiation. *Geochimica Et Cosmochimica Acta* **73**, 729-749.

Huang, F., Zhang, Z., Lundstrom, C. C., and Zhi, X., 2011. Iron and magnesium isotopic compositions of perditotie xenoliths from Eastern China. *Geochimica Et Cosmochimica Acta* **75**, 3318-3334.

Huang, S., Farkas, J., and Jacobsen, S. B., 2010b. Calcium isotopic fractionation between clinopyroxene and orthopyroxene from mantle peridotites. *Earth and Planetary Science Letters* **292**, 337-344.

Ionov, D., 2004. Chemical variations in peridotite xenoliths from Vitim, Siberia: Inferences for REE and Hf behaviour in the garnet-facies upper mantle. *Journal of Petrology* **45**, 343-367.

Ionov, D. A., 2007. Compositional variations and heterogeneity in fertile lithospheric mantle: peridotite xenoliths in basalts from Tariat, Mongolia. *Contributions to Mineralogy and Petrology* **154**, 455-477.

Ionov, D. A., 2010. Petrology of Mantle Wedge Lithosphere: New Data on Supra-Subduction Zone Peridotite Xenoliths from the Andesitic Avacha Volcano, Kamchatka. *Journal of Petrology* **51**, 327-361.

Ionov, D. A., Ashchepkov, I., and Jagoutz, E., 2005a. The provenance of fertile off-craton lithospheric mantle: Sr–Nd isotope and chemical composition of garnet and spinel peridotite xenoliths from Vitim, Siberia *Chemical Geology* **217**, 41-75.

Ionov, D. A., Chanefo, I., and Bodinier, J. L., 2005b. Origin of Fe-rich lherzolites and wehrlites from Tok, SE Siberia by reactive melt percolation in refractory mantle peridotites. *Contributions to Mineralogy and Petrology* **150**, 335-353.

Ionov, D. A., Chazot, G., Chauvel, C., Merlet, C., and Bodinier, J. L., 2006. Trace element distribution in peridotite xenoliths from Tok, SE Siberian craton: A record of pervasive, multi-stage metasomatism in shallow refractory mantle. *Geochimica Et Cosmochimica Acta* **70**, 1231-1260.

Ionov, D. A. and Hofmann, A. W., 2007. Depth of formation of subcontinental off-craton peridotites. *Earth and Planetary Science Letters* **261**, 620-634.

Ionov, D. A., Prikhodko, V. S., Bodinier, J. L., Sobolev, A. V., and Weis, D., 2005c. Lithospheric mantle beneath the south-eastern Siberian craton: petrology of peridotite xenoliths in basalts from the Tokinsky Stanovik. *Contributions to Mineralogy and Petrology* **149**, 647-665.

Ionov, D. A. and Seitz, H. M., 2008. Lithium abundances and isotopic compositions in mantle xenoliths from subduction and intra-plate settings: Mantle sources vs. eruption histories. *Earth and Planetary Science Letters* **266**, 316-331.

Ionov, D. A. and Wood, B. J., 1992. The oxidation state of subcontinental mantle: oxygen thermobarometry of mantle xenoliths from central Asia. *Contributions to Mineralogy and Petrology* **111**, 179-193.

Jambon, A., Carron, J.-P., and Delbove, F., 1978. Lithium diffusion in silicate glasses of albite, orthoclase and obsidian composition: an ion-microprobe determination. *Earth and Planetary Science Letters* **37**, 445-450.

James, R. H. and Palmer, M. R., 2000. The lithium isotope composition of international rock standards. *Chemical Geology* **166**, 319-326.

Jeffcoate, A. B., Elliott, T., Kasemann, S. A., Ionov, D., Cooper, K., and Brooker, R., 2007. Li isotope fractionation in peridotites and mafic melts. *Geochimica Et Cosmochimica Acta* **71**, 202-218.

Jeffcoate, A. B., Elliott, T., Thomas, A., and Bouman, C., 2004. Precise, small sample size determinations of lithium isotopic compositions of geological reference materials and modern seawater by MC-ICP-MS. *Geostandards and Geoanalytical Research* **28**, 161-172.

Kaliwoda, M., Ludwig, T., and Altherr, R., 2008. A new SIMS study of Li, Be, B and d7Li in mantle xenoliths from Harrat Uwayrid (Saudi Arabia). *Lithos* **106**, 261-279.

Kallemeyn, G. W. and Wasson, J. T., 1986. Compositions of enstatite (EH3, EH4,5 and EM) chondrites: Implications regarding their formation *Geochim. Cosmochim. Acta* **50**, 2153-5164.

Kohn, S. C. and Grant, K. J., 2006. The partitioning of water between nominally anhydrous minerals and silicate melts, *Water in Nominally Anhydrous Minerals*.

Lee, T. and Papanastassiou, D. A., 1974. Mg isotopic anomalies in the Allende meteorite and correlation with O and Sr effects. *Geophysical Research Letters* **1**, 225-228.

Lee, T., Papanastassiou, D. A., and Wasserburg, G. J., 1976. Demonstration of 26Mg excess in Allende and evidence for 26Al. *Geophysical Research Letters* **3**, 41-44.

Li, W. Y., Teng, F. Z., Xiao, Y., and Huang, J., 2011. High-temperature inter-mineral magnesium isotope fractionation in eclogite from the Dabie orogen, China. *Earth and Planetary Science Letters* **304**, 224-230.

Liu, S.-A., Teng, F. Z., He, Y., Ke, S., and Li, S., 2010. Investigation of magnesium isotope fractionation during granite differentiation: Implication for Mg isotopic composition of the continental crust. *Earth and Planetary Science Letters* **297**, 475-482.

Lowry, R. K., Henderson, P., and Nolan, J., 1982. Tracer Diffusion of Some Alkali, Alkaline-Earth and Transition Element Ions in a Basaltic and an Andesitic Melt, and the Implications Concerning Melt Structure *Contributions to Mineralogy and Petrology* **80**, 254-261.

Lundstrom, C. C., Chaussidon, M., Hsui, A. T., Kelemen, P., and Zimmerman, M., 2005. Observations of Li isotopic variations in the Trinity Ophiolite: Evidence for isotopic fractionation by diffusion during mantle melting. *Geochimica Et Cosmochimica Acta* **69**, 735-751.

Magna, T., Ionov, D. A., Oberli, F., and Wiechert, U., 2008. Links between mantle metasomatism and lithium isotopes: Evidence from glass-bearing and cryptically metasomatized xenoliths from Mongolia. *Earth and Planetary Science Letters* **276**, 214-222.

Magna, T., Wiechert, U., and Halliday, A. N., 2006a. Lithium isotope composition of the inner solar system materials. *Meteoritics & Planetary Science* **41**, A110-A110.

Magna, T., Wiechert, U., and Halliday, A. N., 2006b. New constraints on the lithium isotope compositions of the Moon and terrestrial planets. *Earth and Planetary Science Letters* **243**, 336-353.

Marschall, H. R., Altherr, R., and Rupke, L., 2007a. Squeezing out the slab — modelling the release of Li, Be and B during progressive high-pressure metamorphism. *Chemical Geology* **239**, 323-335.

Marschall, H. R., Pogge von Strandmann, P. A. E., Seitz, H. M., Elliott, T., and Niu, Y. L., 2007b. The lithium isotopic composition of orogenic eclogites and deep subducted slabs. *Earth and Planetary Science Letters* **262**, 563-580.

McCoy, T. J., Dickinson, T. L., and Lofgren, G. E., 1999. Partial melting of the Indarch (EH4) meteorite: a textural, chemical, and phase relations view of melting and melt migration. *Meteoritics and Planetary Science* **34**, 735-746.

McDonough, W. F., 1990. Constraints on the composition of the continental lithospheric mantle. *Earth and Planetary Science Letters* **101**, 1-18.

McDonough, W. F. and Frey, F. A., 1989. Rare-Earth Elements in Upper Mantle Rocks. In: Lipin, B. R. and McKay, G. A. Eds.), *Geochemistry and Mineralogy of Rare Earth Elements*.

McDonough, W. F. and Sun, S.-s., 1995. The composition of the Earth. *Chemical Geology* **120**, 223-253.

McDonough, W. F., Teng, F. Z., Tomascak, P. B., Ash, R. D., Grossmann, J. N., and Rudnick, R. L., 2003. Lithium isotopic composition of chondritic meteorites. *Lunar and Planetary Science XXXIV*.

Miller, D. P., Marschall, H. R., and Schumacher, J. C., 2009. Metasomatic formation and petrology of blueschist-facies hybrid rocks from Syros (Greece): Implications for reactions at the slab-mantle interface. *Lithos* **107**, 53-67.

Morioka, M., 1981. Cation Diffusion in Olivine .2. Ni-Mg, Mn-Mg, Mg and Ca. *Geochimica Et Cosmochimica Acta* **45**, 1573-1580.

Nishio, Y., Nakai, S., Kogiso, T., and Barsczus, H. G., 2005. Lithium, strontium, and neodymium isotopic compositions of oceanic island basalts in the Polynesian region: constraints on a Polynesian HIMU origin. *Geochemical Journal* **39**, 91-103.

Norman, M. D., Yaxley, G. M., Bennett, V. C., and Brandon, A. D., 2006. Magnesium isotopic composition of olivine from the Earth, Mars, Moon, and pallasite parent body. *Geophysical Research Letters* **33**.

Palme, H. and O'Neill, H. S., 2003. Cosmochemical Estimates of Mantle Composition. In: Davis, A. M., Holland, H. D., and Turekian, K. K. Eds.), *Treatise on Geochemistry*. Elsevier.

Pearson, N. J., Griffin, W. L., Alard, O., and O'Reilly, S. Y., 2006. The isotopic composition of magnesium in mantle olivine: Records of depletion and metasomatism. *Chemical Geology* **226**, 115-133.

Pogge von Strandmann, P. A. E., 2008. Precise magnesium isotope measurements in core top planktic and benthic foraminifera. *Geochem. Geophys. Geosyst.* **9**, Q12015, doi:10.1029/2008GC002209.

Preß, S., Witt, G., Seck, H. A., Ionov, D., and Kovalenko, V. I., 1986. Spine1 peridotite xenoliths from the Tariat Depression, Mongolia. I: Major element chemistry and mineralogy of a primitive mantle xenolith suite. *Geochimica Et Cosmochimica Acta* **50**, 2587-2599.

Qian, Q., O'Neill, H. S., and Hermann, J., 2010. Comparative diffusion coefficients of major and trace elements in olivine at ~950 °C from a xenocryst included in dioritic magma. *Geology* **38**, 331-334.

Richter, F. M., Dauphas, N., and Teng, F. Z., 2009. Non-traditional fractionation of non-traditional isotopes: Evaporation, chemical diffusion and Soret diffusion. *Chemical Geology* **258**, 92-103.

Richter, F. M., Davis, A. M., DePaolo, D. J., and Watson, E. B., 2003. Isotope fractionation by chemical diffusion between molten basalt and rhyolite. *Geochimica Et Cosmochimica Acta* **67**, 3905-3923.

Richter, F. M., Liang, Y., and Davis, A. M., 1999. Isotope fractionation by diffusion in molten oxides. *Geochimica Et Cosmochimica Acta* **63**, 2853-2861.

Richter, F. M., Watson, E. B., Mendybaev, R. A., Teng, F. Z., and Janney, P. E., 2008. Magnesium isotope fractionation in silicate melts by chemical and thermal diffusion. *Geochimica Et Cosmochimica Acta* **72**, 206-220.

Ringwood, A. E., 1975. *Composition and Petrology of the Earth's Mantle*. McGraw-Hill.

Rudnick, R. L. and Ionov, D. A., 2007. Lithium elemental and isotopic disequilibrium in minerals from peridotite xenoliths from far-east Russia: Product of recent melt/fluid–rock reaction. *Earth and Planetary Science Letters* **256**, 278-293.

Ryan, J. G. and Kyle, P. R., 2004. Lithium abundance and lithium isotope variations in mantle sources: insights from intraplate volcanic rocks from Ross Island and Marie Byrd Land (Antarctica) and other oceanic islands. *Chemical Geology (Lithium Isotope Geochemistry)* **212**, 125-142.

Ryan, J. G. and Langmuir, C. H., 1987. The systematics of lithium abundances in young volcanic rocks. *Geochimica Et Cosmochimica Acta* **51**, 1727-1741.

Sanford, R. F., 1982. Growth of Ultramafic Reaction Zones in Greenschist to Amphibolite Facies Metamorphism. *American Journal of Science* **282**, 543-616.

Schiller, M., Baker, J. A., and Bizzarro, M., 2010. 26Al-26Mg dating of asteroidal magmatism in the young Solar System. *Geochimica Et Cosmochimica Acta* **74**, 4844-4864.

Schultz, L. and Franke, L., 2004. Helium, neon, and argon in meteorites: A data collection. *Meteoritics and Planetary Science* **39**, 1889-1890.

Seitz, H.-M., Brey, G. P., Lahaye, Y., Durali, S., and Weyer, S., 2004. Lithium isotopic signatures of peridotite xenoliths and isotopic fractionation at high temperature between olivine and pyroxenes. *Chemical Geology (Lithium Isotope Geochemistry)* **212**, 163-177.

Seitz, H. M., Brey, G. P., Zipfel, J., Ott, U., Weyer, S., Durali, S., and Weinbruch, S., 2007. Lithium isotope composition of ordinary and carbonaceous chondrites, and differentiated planetary bodies: Bulk solar system and solar reservoirs. *Earth and Planetary Science Letters* **260**, 582-596.

Seitz, H. M. and Woodland, A. B., 2000. The distribution of lithium in peridotitic and pyroxenitic mantle lithologies - an indicator of magmatic and metasomatic processes. *Chemical Geology* **166**, 47-64.

Sephton, M. A., James, R. H., and Bland, P. A., 2004. Lithium isotope analyses of inorganic constituents from the Murchison Meteorite. *The Astrophysical Journal* **612**, 588-591.

Sephton, M. A., James, R. H., and Zolensky, M. E., 2006. The origin of dark inclusions in Allende: New evidence from lithium isotopes. *Meteoritics & Planetary Science* **41**, 1039-1043.

Shannon, R. D. and Prewitt, C. T., 1969. Effective Ionic Radii in Oxides and Fluorides. *Acta Crystallographica* **B25**, 925-946.

Spandler, C. and O'Neill, H. S., 2010. Diffusion and partition coefficients of minor and trace elements in San Carlos olivine at 1,300A degrees C with some geochemical implications. *Contributions to Mineralogy and Petrology* **159**, 791-818.

Sun, S.-s., 1982. Chemical composition and origin of the earth's primitive mantle. *Geochimica Et Cosmochimica Acta* **46**, 179-192.

Svanson, S. E. and Johansson, R., 1970. A Nuclear Magnetic Resonance Study of Diffusion in Lithium Silicate Glasses. *Acta Chemica Scandinavica* **24**, 755-774.

Tang, Y.-J., Zhang, H. F., Nakamura, E., Moriguti, T., Kobayashi, K., and Ying, J.-F., 2007. Lithium isotopic systematics of peridotite xenoliths from Hannuoba, North China Craton: Implications for melt–rock interaction in the considerably thinned lithospheric mantle. *Geochimica Et Cosmochimica Acta* **71**, 4327-4341.

Teng, F.-Z., Wadhwa, M., and Helz, R. T., 2007. Investigation of magnesium isotope fractionation during basalt differentiation: Implications for a chondritic composition of the terrestrial mantle. *Earth and Planetary Science Letters* **261**, 84-92.

Teng, F. Z., Li, W. Y., Ke, S., Marty, B., Dauphas, N., Huang, S., Wu, F.-Y., and Pourmand, A., 2010. Magnesium isotopic composition of the Earth and chondrites. *Geochimica Et Cosmochimica Acta* **74**, 4150-4166.

Teng, F. Z., McDonough, W. F., Rudnick, R. L., and Walker, R. J., 2006. Diffusion-driven extreme lithium isotopic fractionation in country rocks of the Tin Mountain pegmatite. *Earth and Planetary Science Letters* **243**, 701-710.

Thrane, K., Nagashima, K., Krot, A. N., and Bizzarro, M., 2008. Discovery of a new FUNCAI from a CV carbonaceous chondrite: Evidence for multistage thermal

processing in the protoplanetary disk. *Astrophysical Journal Letters* **680**, L141-L144.

Tipper, E. T., Galy, A., and Bickle, M. J., 2006a. Riverine evidence for a fractionated reservoir of Ca and Mg on the continents: Implications for the oceanic Ca cycle. *Earth and Planetary Science Letters* **247**, 267-279.

Tipper, E. T., Galy, A., Gaillardet, J., Bickle, M. J., Elderfield, H., and Carder, E. A., 2006b. The magnesium isotope budget of the modern ocean: Constraints from riverine magnesium isotope ratios. *Earth and Planetary Science Letters* **250**, 241-253.

Tipper, E. T., Louvat, P., Capmas, F., Galy, A., and Gaillardet, J., 2008. Accuracy of stable Mg and Ca isotope data obtained by MC-ICP-MS using the standard addition method. *Chemical Geology* **257**, 65-75.

Tomascak, P. B., 2004. Developments in the understanding and application of lithium isotopes in the earth and planetary sciences, *Geochemistry of Non-Traditional Stable Isotopes*.

Tomascak, P. B., Ryan, J. G., and Defant, M. J., 2000. Lithium isotope evidence for light element decoupling in the Panama subarc mantle. *Geology* **28**, 507-510.

Tomascak, P. B., Widom, E., Benton, L. D., Goldstein, S. L., and Ryan, J. G., 2002. The control of lithium budgets in island arcs. *Earth and Planetary Science Letters* **196**, 227-238.

Wang, J., Davis, A. M., Clayton, R. N., and Hashimoto, A., 1999. Evaporation of single crystal forsterite: evaporation kinetics, magnesium isotope fractionation, and implications of mass-dependent isotopic fractionation of a diffusion-controlled reservoir. *Geochimica Et Cosmochimica Acta* **63**, 953-966.

Weyer, S. and Ionov, D. A., 2007. Partial melting and melt percolation in the mantle: The message from Fe isotopes. *Earth and Planetary Science Letters* **259**, 119-133.

Wiechert, U., Ionov, D. A., and Wedepohl, K. H., 1997. Spinel peridotite xenoliths from the Atsagin-Dush volcano, Dariganga lava plateau, Mongolia: a record of partial melting and cryptic metasomatism in the upper mantle. *Contributions to Mineralogy and Petrology* **126**, 345-364.

Wiechert, U. H. and Halliday, A. N., 2007. Non-chondritic magnesium and the origins of the inner terrestrial planets. *Earth and Planetary Science Letters* **256**, 360-371.

Woodland, A. B., Seitz, H. M., Yaxley, G. M., and Altherr, R., 2002. Li as an indicator of petrogenetic processes in the Earth's mantle. *Geochimica Et Cosmochimica Acta* **66**, A846-A846.

Workman, R. K. and Hart, S. R., 2005. Major and trace element composition of the depleted MORB mantle (DMM). *Earth and Planetary Science Letters* **231**, 53-72.

Yamada, M., Tachibana, S., Nagahara, H., and Ozawa, K., 2006. Anisotropy of Mg isotopic fractionation during evaporation and Mg self-diffusion of forsterite in vacuum. *Planetary and Space Science* **54**, 1096-1106.

Yang, W., Teng, F. Z., and Zhang, H. F., 2009. Chondritic magnesium isotopic composition of the terrestrial mantle: A case study of peridotite xenoliths from the North China craton. *Earth and Planetary Science Letters* **288**, 475-482.

Young, E. D., Ash, R. D., Galy, A., and Belshaw, N. S., 2002. Mg isotope heterogeneity in the Allende meteorite measured by UV laser ablation-MC-

ICPMS and comparisons with O isotopes. *Geochimica Et Cosmochimica Acta* **66**, 683-698.

Young, E. D. and Galy, A., 2004. The isotope geochemistry and cosmochemistry of magnesium. In: Johnson, C. M., Beard, B. L., and Albarede, F. Eds.), *Geochemistry of non-traditional stable isotopes*. Mineralogical Society of America, Geochemical Society.

Young, E. D., Tonui, E., Manning, C. E., Schauble, E., and Macris, C. A., 2009. Spinel–olivine magnesium isotope thermometry in the mantle and implications for the Mg isotopic composition of Earth. *Earth and Planetary Science Letters* **288**, 524-533.

Zindler, A. and Jagoutz, E., 1988. Mantle cryptology. *Geochimica Et Cosmochimica Acta* **52**, 319-333.

Figure captions

Figure 1. Primitive mantle normalised (Sun, 1982) La/Sm ratios plotted against Mg#, molar Mg/[Fe(II)+Mg], for all analysed peridotites. Samples are plotted according to geodynamic locality. Data sources are as follows: off-craton peridotites (Tariat and Dariganga) Ionov (2007), Ionov and Hofmann (2007); (Vitim) Ionov et al. (2005a); arc peridotites (Avacha) Ionov (2010); cratonic peridotites and wehrlites (Tok) Ionov et al. (2005a), Ionov et al. (2005b). Solid black points are those taken as representative of the fertile mantle (see text for details). The stars show compositions for primitive mantle (PM) and depleted MORB mantle (DMM) taken from Sun, 1982, McDonough and Frey, 1989, Workman and Hart, 2005.

Figure 2. Measured δ^{26}Mg (±2se) of the DSM-3 standard doped with variable amounts of Ni plotted against Mg/Ni (weight ratio) of mixture to investigate a possible matrix influence. No effect is evident.

Figure 3. Compilation of analyses of USGS standards both measured by different protocols in this study and by others. Open diamonds represent analyses from this study. Open circles are published data. (1) Wiechert et al., 2007; (2) Handler et al., 2009; (3) Huang et al., 2011; (4) Bourdon et al., 2010; (5) Huang et al., 2009; (6) Wombacher et al., 2009; (7) Tipper et al., 2008; (8) Teng et al., 2007; (9) Baker et al., 2005; (10) Bizzarro et al., 2005; (11) Bizzarro et al., 2011; (12) Pogge von Strandmann et al., 2008. Error bars represent the external uncertainty (2sd) reported by each study.

Figure 4. (a) δ^{7}Li vs. [Li] for bulk meteorite samples. The error bars indicate the 2s.d. external uncertainty of the procedure used in this study. The small grey symbols represent data from other studies (James and Palmer, 2000; Sephton et al., 2004, 2006; Magna et al., 2006; Seitz et al., 2007). Two eucrites, with high [Li], plot off scale. (b) Bulk chondrite δ^{7}Li vs. δ^{26}Mg data from this study.

Figure 5. a) δ^{7}Li vs. [Li] for the bulk xenolith samples. The grey box represents the range of this study's chondrite analyses. The error bars represent the 2s.d. external uncertainty of the analyses. The small grey symbols represent published whole-rock or reconstituted whole-rock data (Brooker et al., 2004; Seitz et al., 2004; Magna et al., 2006; Jeffcoate et al., 2007; Magna et al., 2008; Aulbach et al., 2009). Solid black points are those taken as representative of the fertile mantle (see discussion for details). b) Bulk peridotite δ^{26}Mg as a function of Mg#. The error bars represent the 2s.d. external uncertainty of the analyses. The small grey symbols represent published whole-rock data (Wiechert et al., 2007; Yang et al., 2009; Teng et al., 2010, Bourdon et al., 2010; Chakrabarti et al., 2010; Huang et al., 2011). Solid black points are those taken as representative of the fertile mantle (see discussion for details).

Figure 6. (a) Difference in δ^{26}Mg between coexisting olivine and clinopyroxene, as a function of whole rock δ^{26}Mg. Legend as in Fig. 5. The dashed lines represent the theoretical fractionations, as calculated by Young et al., 2009, for the temperature range inferred from major element geothermometry of the xenoliths studied. (b) Difference in δ^{7}Li between coexisting olivine and

clinopyroxene, as a function of whole-rock δ^7Li. Where not measured by this study, data were taken from Rudnick and Ionov, 2007, Jeffcoate et al., 2007, Ionov and Seitz, 2008, Magna et al., 2006.

Figure 7. Standard addition plot of JP-1 mixtures with CAM-1, showing that JP-1 is not as isotopically heavy as suggested by Wiechert and Halliday (2007). See text for details. Error ellipses represent the 2s.d. of the samples (black ellipses), and the 2s.d. of JP-1 and CAM-1 (grey ellipses). Regression and error parabola were calculated using formulae from York (1966).

Figure 8. Co-variation between δ^7Li and δ^{26}Mg for the bulk xenoliths. The light grey box represents the range of this study's chondrite analyses. The error bars represent the 2s.d. external uncertainty of the analyses. Solid black points are those taken as representative of the fertile mantle (see discussion for details).

Figure 9. Modelled bulk xenolith isotope ratios as a function of cooling time. Model parameters are as shown in Figure 10.

Figure 10. Modelled covariation of Li and Mg isotope ratios by diffusional fractionation. The legend provides details of the β, relative diffusivities and activity gradients used in the calculations See text for model details. Li diffusivity (D_{Li}) is from Dohmen et al. (2010) at ~1250°C. β_{Li} is from Richter et al. (2003), and β_{Mg} is the best-fit value. Symbols as in Figure 5.

Figure 11. (a) δ^7Li as a function of [Li] for the Avacha xenoliths. The error bars represent the 2s.d. external uncertainty of the analyses. Open symbols represent analytical repeats. (b) Avacha δ^7Li data as a function of FeO.

		Li (ppm)	FeO total (wt%)	MgO (wt%)	Mg#	δ^7Li (‰)	2s.e.	δ^{25}Mg (‰)	2s.e.	δ^{26}Mg (‰)	2s.e.	Δ^{25}Mg (‰)	δ^{26}Mg* (‰)	sample weight (g)	Emplacement
Chondrites															
Carbonaceous chondrites															
Orgueil (BM.36104)	CI1	1.2				4.1	0.1	-0.08	0.01	-0.15	0.02	0.00	0.0023	0.01289	
Orgueil	CI1	1.5				2.6	0.1								
Karoonda (BM.1931,489)	CK4	0.9				3.8	0.1	-0.16	0.01	-0.31	0.01	0.00	0.0060	0.01201	
Murchison (BM.1970,6)	CM2	1.0				3.4	0.04	-0.13	0.01	-0.23	0.02	-0.01	0.0109	0.02401	
Murchison	CM2	1.5				4.4	0.2								
Kainsaz (BM.1965,395)	CO3.2	1.4				3.5	0.03	-0.16	0.01	-0.28	0.01	-0.01	0.0250	0.02378	
Ornans	CO	1.3				3.1	0.2								
Felix	CO3	1.2				3.1	0.1								
NWA 801*	CR2	0.7				1.6	0.1								
Allende (BM.1988,M24)	CV3	1.2				2.7	0.1	-0.19	0.02	-0.36	0.02	0.00	0.0001	0.02002	
rpt							0.2	-0.19	0.02	-0.37	0.03	0.00		0.01022	
Allende chondrule		1.3				-0.3	0.2								
Leoville	CV3	1.7				2.3	0.04								
Ordinary chondrites															
Barratta* (BM.1989,M31)	L4	1.8				2.5	0.04	-0.16	0.01	-0.32	0.01	0.00	-0.0030	0.03821	
Tenham (BM.1935,785)	L6	1.1				2.4	0.2	-0.13	0.01	-0.26	0.03	0.00	-0.0030	0.02126	
Barwell	L6	1.5				3.0	0.1								
Chainpur	LL3	2.1				2.4	0.03								
Parnallee (BM.34792)	LL3.6	1.5				3.9	0.2	-0.19	0.01	-0.38	0.01	0.01	0.0025	0.01608	
Parnallee	LL3.6	1.8				2.7	0.1								
Dhurmsala (BM.96262)	LL6	1.1				2.7	0.02	-0.15	0.02	-0.28	0.02	0.00	0.0072	0.03433	
Ceniceros (BM.1989,M31)	H3.7	1.2				2.4	0.1	-0.15	0.01	-0.28	0.02	0.00	-0.0001	0.02239	
Butsura (BM.34795)	H6	1.8				2.5	0.1	-0.09	0.01	-0.18	0.03	0.00	-0.0060	0.03393	
rpt						3.0	0.1							0.01015	
Ogi	H6 (W2)	1.4				1.6	0.2								
Tieschitz	H/L3	1.4				4.3	0.1								
Enstatite chondrites															
Indarch (BM.1921,23)	EH4	2.2				2.0	0.1	-0.12	0.01	-0.21	0.01	-0.01	0.0016	0.02288	
Abee (BM.1997,M7)	EH4	1.6				2.8	0.2	-0.14	0.01	-0.27	0.01	0.00	0.0068	0.01254	
St. Mark's (BM.1970,339)	EH5	1.3				0.5	0.1	-0.17	0.01	-0.33	0.02	0.00	-0.0018	0.01842	
rpt								-0.14	0.02	-0.25	0.02	0.00		0.00844	
Daniel's Kuil	EL6					1.7	0.2								
Khairpur (BM.51366)	EL6	1.6				1.2	0.1	-0.12	0.02	-0.22	0.03	0.00	0.0040	0.01414	
Yilmia* (BM.1972,132)	EL6	1.2				2.1	0.1	-0.11	0.01	-0.23	0.01	0.01	-0.0154	0.01390	
Hvittis (BM.86754)	EL6	1.7				1.5	0.2	-0.15	0.01	-0.27	0.02	-0.01	0.0125	0.00934	
Achondrites															
Khor Temiki	Aubrite	0.6				-0.3	0.1								
Stannern	Eucrite					3.4	0.2								
Pasamonte	Eucrite	12.2				3.7	0.1								
Camel Donga	Eucrite	7.2				2.8	0.1								
Peridotites															
Tariat															
4500-19d	sp hrz	0.5	7.60	45.78	0.915	-1.6	0.1	-0.17	0.01	-0.34	0.02	0.01	0.0083		?
Mo-101	sp lhz	1.6	8.04	37.17	0.892	2.6	0.2	-0.14	0.01	-0.26	0.02	-0.01	-0.0121		?
Hr-25	sp lhz	1.2	13.10	35.35	0.828	4.9	0.2	-0.09	0.01	-0.16	0.01	-0.01	0.0188		P
4500-18	sp hrz	1.3	7.28	46.56	0.919	-3.9	0.1	-0.17	0.01	-0.35	0.01	0.01	0.0170		?
rpt						-3.6	0.1	-0.18	0.01	-0.38	0.02	0.01	0.0167		
8531-40	sp hrz	3.8	8.80	44.63	0.900	1.8	0.1	-0.15	0.02	-0.29	0.01	0.00	0.0171		?
8530-24	sp hrz	1.5	8.85	43.57	0.898	2.1	0.1	-0.13	0.01	-0.25	0.02	-0.01	0.016		?
Z-9	sp lhz	2.1	9.32	40.76	0.886	3.5	0.1	-0.06	0.01	-0.13	0.02	0.01	-0.0092		P
4230-16	phl sp lhz	1.8	8.4	36.94	0.887	3.9	0.2	-0.11	0.01	-0.21	0.01	0.00	0.0036		P
rpt						3.8	0.1	-0.10	0.01	-0.19	0.01	0.00			
Dariganga															
BN-8	sp hrz	0.9	7.13	45.21	0.919	2.0	0.1	-0.11	0.01	-0.22	0.01	0.00	-0.0183		P
8505-2	sp hrz	1.6		46.00	0.915	3.3	0.2	-0.06	0.01	-0.16	0.01	0.02	-0.0011		P
Vitim															
314-56	sp lhz	1.9	8.38	37.18	0.888	3.7	0.2	-0.09	0.02	-0.19	0.01	0.01	0.0115		P
313-102	grt lhz	1.6	8.16	37.05	0.884	3.3	0.01	-0.11	0.01	-0.22	0.01	0.00	0.0149		P
314-58	sp lhz	1.2	8.23	38.58	0.893	2.5	0.1	-0.11	0.01	-0.21	0.01	0.00	-0.0108		P
313-105	grt lhz	1.9	8.12	40.37	0.899	2.5	0.1	-0.12	0.01	-0.23	0.01	0.00	0.0165		P
Avacha															
Av-1	sp hrz	1.7	8.11	45.56	0.909	6.0	0.1	-0.08	0.01	-0.14	0.01	-0.01	0.0176		P
rpt		1.7				5.9	0.2	-0.08	0.01	-0.15	0.01	-0.01	0.0092		
Av-4	sp hrz	1.0	8.07	43.73	0.906	4.2	0.2	-0.09	0.01	-0.16	0.02	0.00	0.0191		P
Av-6	sp hrz	1.6	8.24	45.97	0.909	5.4	0.1	-0.03	0.01	-0.06	0.01	0.00	0.0194		
rpt								-0.06	0.01	-0.13	0.01	0.01			P
Av-8	sp hrz	1.3	7.74	44.50	0.911	3.9	0.2	-0.10	0.02	-0.19	0.02	0.00	0.0123		
rpt								-0.12	0.01	-0.23	0.01	0.00			P
Av-16	sp hrz	1.1	7.55	46.20	0.916	2.5	0.1	-0.14	0.01	-0.26	0.01	-0.01	0.0167		
rpt								-0.11	0.01	-0.20	0.01	0.00			P
rpt		1.1				2.7	0.2	-0.13	0.01	-0.25	0.02	0.00	-0.0056		
Av-17	sp hrz	1.3	7.83	46.54	0.914	3.3	0.1	-0.10	0.01	-0.19	0.01	-0.01	0.0212		
rpt		1.3				3.0	0.04	-0.12	0.01	-0.23	0.01	0.00	-0.0088		P
Tok															
Lherzolite-Harzburgite series															
Tok 2-9	hrz	2.1	7.76	45.78	0.913	4.7	0.2	-0.13	0.01	-0.26	0.01	0.00	-0.0078		F
Tok 6-0	hrz	2.7	7.32	46.31	0.919	-2.5	0.1	-0.16	0.01	-0.31	0.02	0.00	0.0196		F
rpt		2.7				-2.6	0.1	-0.15	0.01	-0.28	0.01	-0.01	-0.0021		
Tok 6-1	lhz	1.4	8.32	38.02	0.891	2.9	0.2	-0.07	0.01	-0.15	0.01	0.01	-0.0109		F
rpt		1.4				2.5	0.02	-0.08	0.01	-0.15	0.02	0.00	0.0142		
Tok 6-3	lhz	2.4	7.39	40.31	0.907	-3.1	0.03	-0.16	0.01	-0.33	0.01	0.01	-0.0055		F
Tok 10-2	hrz	3.1	7.60	45.66	0.915	1.7	0.2	-0.12	0.02	-0.25	0.01	0.00	0.0138		F
Lherzolite-Wehrlite series															
Tok 2-3	low-opx lhz	2.9	9.95	41.05	0.880	2.3	0.1	-0.09	0.01	-0.20	0.01	0.01	-0.0221		F
Tok 2-10	low-opx lhz	2.9	9.43	37.70	0.877	-2.2	0.1	-0.15	0.01	-0.29	0.01	0.00	0.0084		F
Tok 3-2	low-opx lhz	2.3	9.35	41.87	0.889	4.6	0.1	-0.08	0.01	-0.15	0.01	0.00	-0.0166		F
Tok 3-22	whl	3.1	11.82	40.52	0.859	1.2	0.04	-0.14	0.01	-0.28	0.01	0.00	-0.0196		F
Tok 8-10	whl	3.1	9.94	40.68	0.879	4.3	0.1	-0.08	0.01	-0.18	0.01	0.01	-0.0145		F
Tok 10-1	whl	4.8	11.78	36.86	0.848	8.1	0.2	-0.01	0.01	0.00	0.01	-0.01	0.0218		F
rpt						7.9	0.1	0.04	0.02	0.06	0.01	0.00			
Tok 10-3	whl	3.3	13.53	39.47	0.839	2.0	0.2	-0.07	0.01	-0.16	0.01	0.01	-0.0112		F
Tok 10-11	lhz	2.2	14.38	39.09	0.829	4.4	0.1	-0.10	0.01	-0.20	0.01	0.00	0.0158		F
rpt								-0.08	0.01	-0.16	0.01	0.00			

Table 1. Results from measured whole-rock peridotites and meteorites. Peridotite FeO, MgO and Mg# data from Mongolia: Ionov (2007), Ionov and Hofmann (2007); Vitim: Ionov et al. (2005a); Avacha: Ionov (2010); Tok: Ionov et al. (2005a), Ionov et al. (2005b). Repeats reported are the results of complete re-analysis, including re-dissolution. Chondrite $\delta^{26}Mg^*$ data are internally normalised, using $^{25}Mg/^{24}Mg = 0.12663$ and externally normalised to bracketing DSM-3. Sample weights are given for meteorites (see discussion on heterogeneity), but not for terrestrial samples. For the latter, several kg were crushed, and therefore small-scale heterogeneity is not an issue.

*: denotes Find

Emplacement type: P = pyroclastic; F = lava flow

Standard	dissolutions	n	δ^7Li (‰)	2sd
JP-1	11	11	3.0	0.2
BHVO-2	26	31	4.7	0.2
BCR-2	17	18	2.6	0.3
JB-2	24	28	4.9	0.3

Standard	Reference	Introduction method	Chemistry	dissolutions	n	δ^{25}Mg (‰)	2sd	δ^{26}Mg (‰)	2sd
JP-1	This study	Qtz spray chamber	HCl	3	6	**-0.12**	**0.04**	**-0.25**	**0.04**
		Qtz spray chamber	HNO_3	11	19	**-0.13**	**0.05**	**-0.25**	**0.05**
		Apex	HNO_3	12	12	**-0.12**	**0.04**	**-0.24**	**0.05**
		Aridus (med. res.)	HNO_3	1	2	**-0.12**	**0.02**	**-0.23**	**0.03**
	Handler et al., 2009				7	**-0.12**	**0.02**	**-0.23**	**0.03**
	Wiechert & Halliday, 2007					+0.03		?	
BHVO-2	This study	Qtz spray chamber	HCl	1	4	**-0.14**	**0.04**	**-0.26**	**0.06**
		Qtz spray chamber	HNO_3	11	21	**-0.12**	**0.05**	**-0.24**	**0.06**
		Apex	HNO_3	7	8	**-0.13**	**0.03**	**-0.24**	**0.05**
	Bizzarro et al., 2011				10	-0.10	0.03	-0.19	0.07
	Pogge von Strandmann et al., 2008					-0.13	0.08	-0.25	0.11
	Wiechert & Halliday, 2007				7	-0.06	0.04	-0.14	0.08
	Bizzarro et al., 2005				9	-0.08	0.06	-0.16	0.10
BCR-2	This study	Qtz spray chamber	HNO_3	5	8	**-0.13**	**0.03**	**-0.25**	**0.06**
		Apex	HNO_3	6	6	**-0.13**	**0.04**	**-0.26**	**0.05**
	Huang et al., 2011					?		-0.34	0.12
	Bourdon et al., 2010				29	-0.06	0.02	-0.12	0.04
	Huang et al., 2009				18	-0.14	0.08	-0.30	0.11
	Wombacher et al., 2009				4	-0.07	0.06	-0.14	0.11
	Tipper et al., 2008					-0.09	0.05	-0.16	0.11
	Teng et al., 2007				28	-0.16	0.09	-0.30	0.08
	Baker et al., 2005				15	-0.09	0.07	-0.19	
	Bizzarro et al., 2005				7	-0.09	0.17	-0.17	0.35
JB-2	This study	Qtz spray chamber	HCl	2	4	**-0.13**	**0.04**	**-0.24**	**0.05**
		Qtz spray chamber	HNO_3	8	14	**-0.11**	**0.02**	**-0.21**	**0.04**
		Apex	HNO_3	6	7	**-0.11**	**0.03**	**-0.21**	**0.05**
	Pogge von Strandmann et al., 2008					-0.12	0.08	-0.24	0.12
	Wiechert & Halliday, 2007				5	-0.09	0.02	-0.18	0.04
	Bizzarro et al., 2005				8	-0.08	0.07	-0.15	0.13
CAM-1	This study	Qtz spray chamber			43	**-1.35**	**0.03**	**-2.62**	**0.04**
			HNO_3		5	**-1.38**	**0.03**	**-2.65**	**0.05**
		Apex			45	**-1.36**	**0.02**	**-2.63**	**0.04**
			HNO_3		2	**-1.37**	**0.04**	**-2.63**	**0.05**
		Aridus (med. res.)			8	**-1.35**	**0.04**	**-2.59**	**0.06**
	Huang et al., 2011					?		-2.63	0.11
	Chakrabarti and Jacobsen 2010					-1.33	0.14	-2.61	0.28
	Pogge von Strandmann, 2008					-1.38	0.06	-2.64	0.08
	Tipper et al., 2008					-1.34	0.05	-2.59	0.08
	Pogge von Strandmann et al., 2008					-1.42	0.10	-2.78	0.15
	Tipper et al., 2006					-1.34	0.08	-2.60	0.14
	Pearson et al., 2006					-1.33	0.07	-2.58	0.14
Std. add. results									
f (JP-1)									
0.70					1	-0.96	0.03	-1.89	0.05
0.51					1	-0.74	0.01	-1.44	0.01
0.30					1	-0.46	0.03	-0.89	0.05

Table 2. Measured standard data for Li and Mg isotopes. Mg isotope results from other studies are also reported, as are results from our standard addition experiment. The number of mass spectrometer analyses is represented by "n",

whereas “dissolutions” represent complete re-analysis, including dissolution and chemistry.

			δ^7Li (‰)	2s.e.	Li (ppm)		
Av1	sp hrz						
		olivine	5.4	0.2	1.4		
		opx	5.8	0.1	1.2		
Av6	sp hrz						
		olivine	5.1	0.1	1.7		
		opx	5.6	0.2	0.7		
		cpx	4.7	0.2	1.0		
		calc. w.r.	5.1	0.1	1.5		
			δ^{25}Mg (‰)	2s.e.	δ^{26}Mg (‰)	2s.e.	Δ^{25}Mg
Tok 6-3	lhz						
		olivine	-0.18	0.01	-0.36	0.02	0.01
		opx	-0.16	0.01	-0.29	0.01	-0.01
		cpx	-0.13	0.02	-0.25	0.01	0.00
		calc. w.r.	-0.17	0.01	-0.34	0.01	0.00
Tok 10-1	whl						
		olivine	-0.03	0.01	-0.06	0.01	0.00
		olivine	-0.06	0.01	-0.10	0.01	-0.01
		opx	0.01	0.01	0.02	0.01	0.00
		opx	0.00	0.01	-0.02	0.02	0.01
		cpx	0.13	0.01	0.25	0.01	0.00
		cpx	0.11	0.01	0.20	0.01	0.01
		calc. w.r.	-0.02	0.01	-0.05	0.01	0.01
Tok 10-11	lhz						
		olivine	-0.11	0.01	-0.20	0.01	-0.01
		olivine	-0.07	0.01	-0.14	0.01	0.00
		opx	-0.05	0.02	-0.12	0.02	0.01
		opx	-0.03	0.01	-0.05	0.01	0.00
		cpx	0.00	0.01	-0.01	0.01	0.00
		cpx	0.00	0.01	0.00	0.01	0.00
		calc. w.r.	-0.08	0.01	-0.16	0.02	0.00
Av6	sp hrz						
		olivine	-0.05	0.01	-0.11	0.01	0.01
		opx	-0.02	0.02	-0.05	0.02	0.01
		cpx	-0.03	0.01	-0.07	0.01	0.01
4230-16	phl sp lhz						
		olivine	-0.11	0.01	-0.23	0.01	0.01
		olivine	-0.10	0.01	-0.20	0.02	0.00
		opx	-0.12	0.02	-0.25	0.02	0.01
		opx	-0.13	0.01	-0.26	0.01	0.00
		cpx	-0.05	0.01	-0.09	0.01	0.00
		cpx	-0.05	0.01	-0.10	0.01	0.00
		calc. w.r.	-0.10	0.01	-0.21	0.01	0.01
314-56	sp lhz						
		olivine	-0.11	0.01	-0.23	0.01	0.01
		olivine	-0.10	0.01	-0.19	0.02	0.00
		opx	-0.09	0.01	-0.21	0.01	0.02
		opx	-0.13	0.01	-0.25	0.01	0.00
		cpx	-0.03	0.01	-0.05	0.01	-0.01
		cpx	-0.03	0.01	-0.06	0.01	0.00
Mo-101	sp lhz						
		olivine	-0.12	0.01	-0.25	0.01	0.01
		olivine	-0.14	0.02	-0.30	0.02	0.01
		opx	-0.11	0.01	-0.23	0.01	0.01
		opx	-0.14	0.01	-0.25	0.01	-0.01
		cpx	-0.09	0.01	-0.18	0.01	0.00
		cpx	-0.06	0.01	-0.13	0.01	0.01
		calc. w.r.	-0.11	0.01	-0.24	0.02	0.01
San Carlos							
		olivine	-0.14	0.01	-0.27	0.01	0.02
		olivine	-0.17	0.01	-0.34	0.01	0.00

Table 3. Mineral separate isotope data. Listed repeats are full dissolution and chemical repeats. The calculated whole rock isotope ratios are given when all mineral abundances and concentrations are known (see Table 1 caption for references).

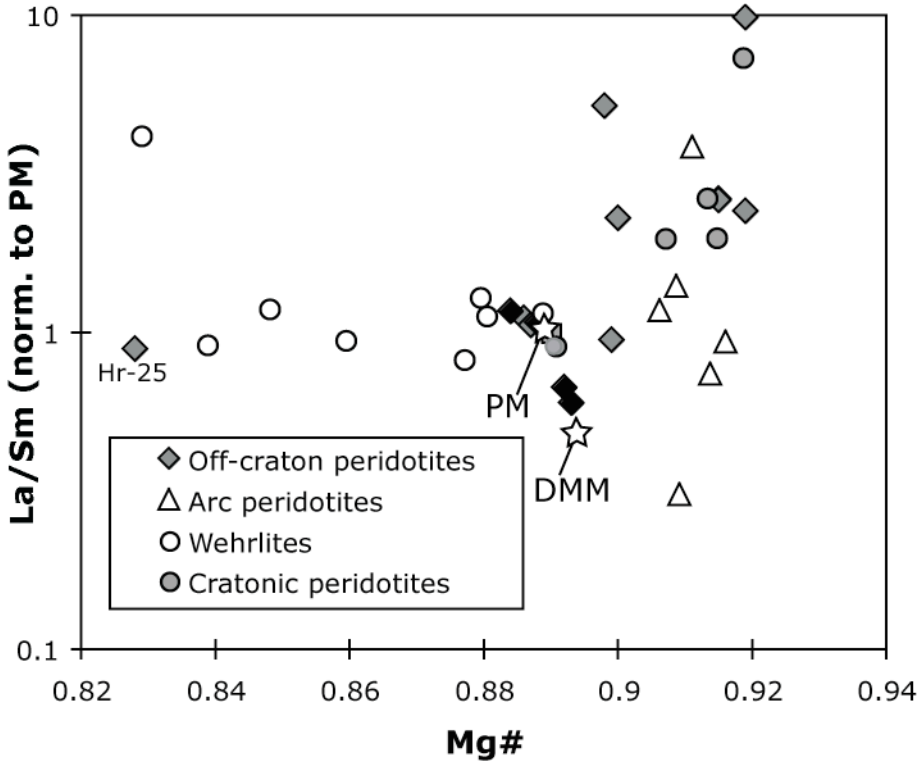

Figure 1

Figure 1

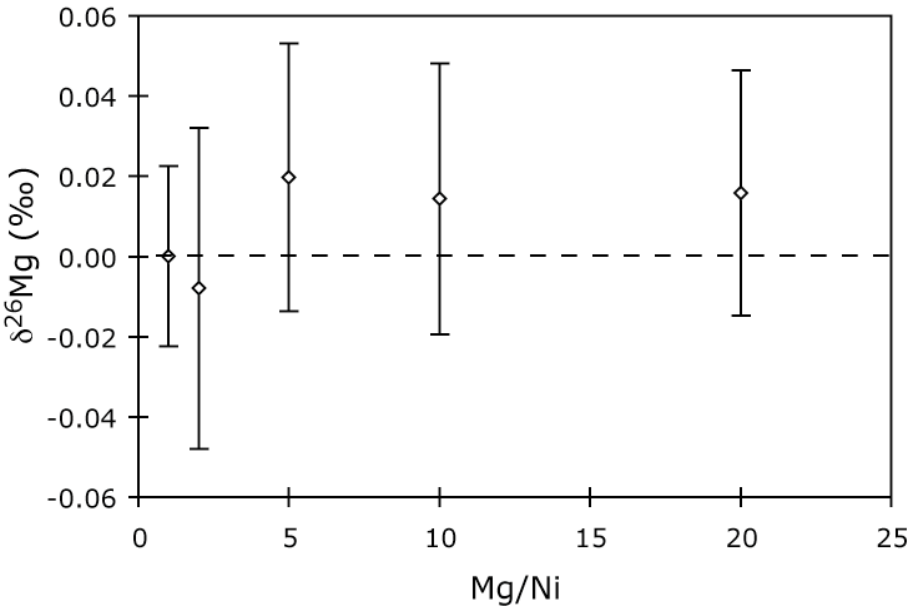

Figure 2

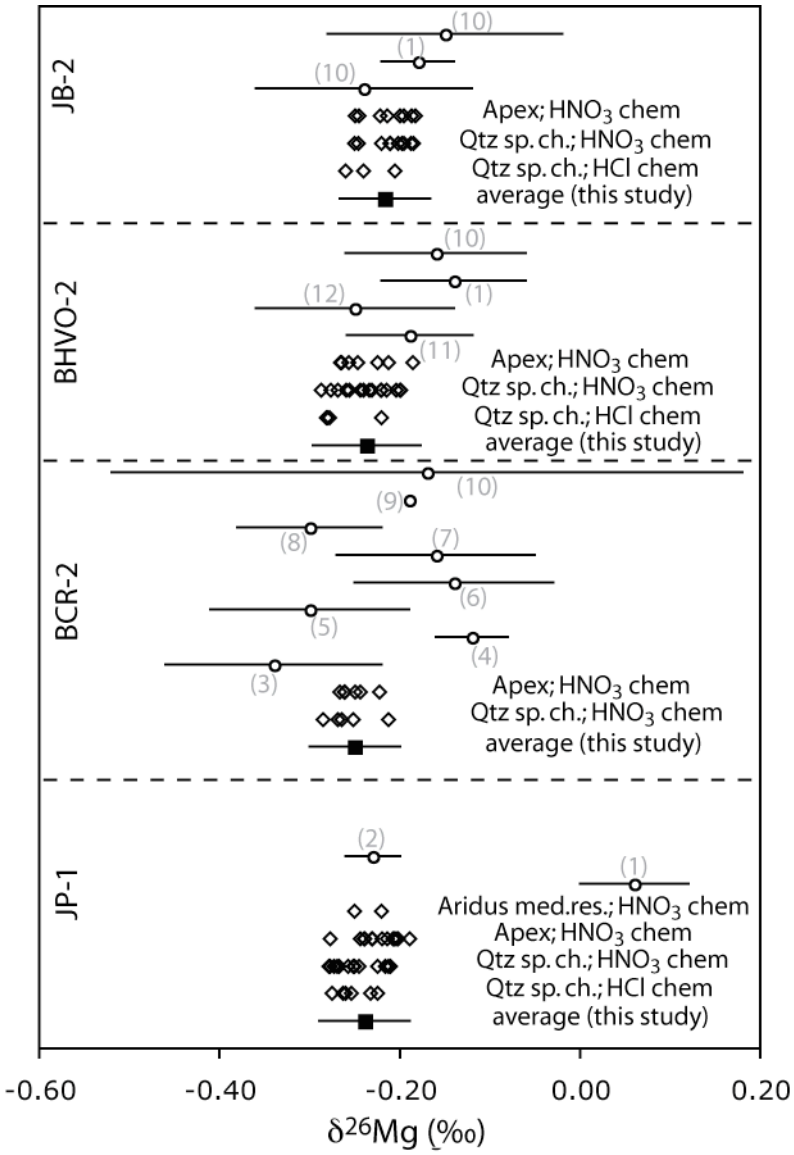

Figure 3

Figure 3

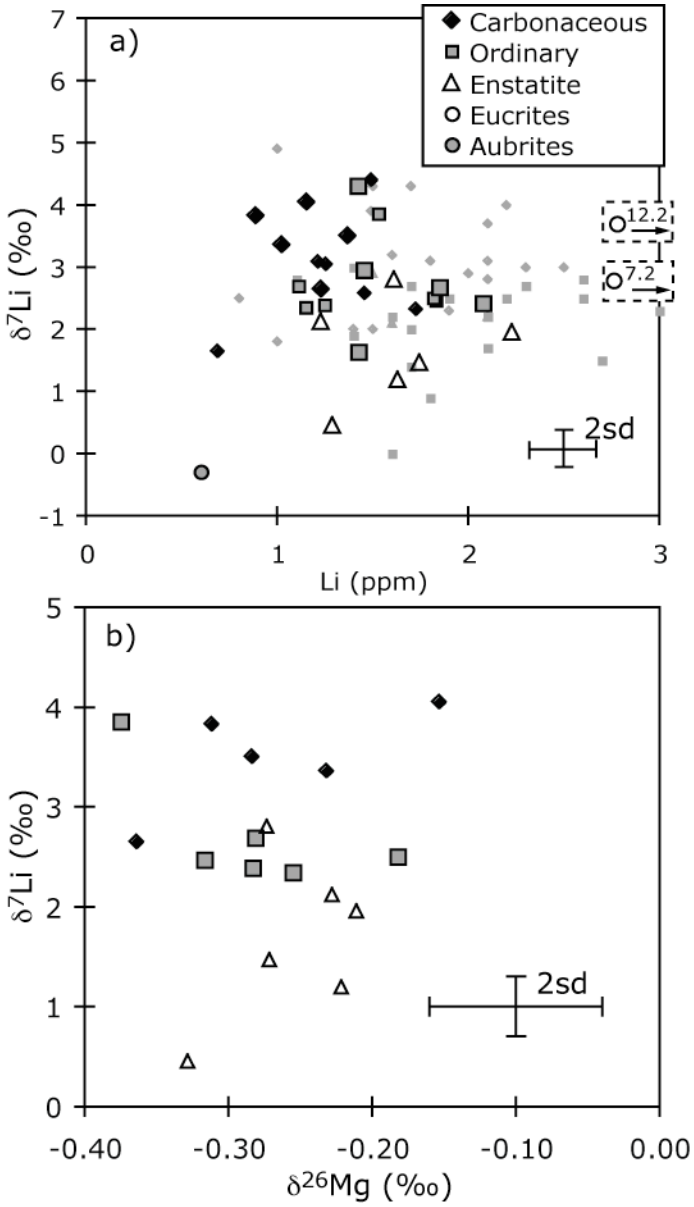

Figure 4

Figure 4

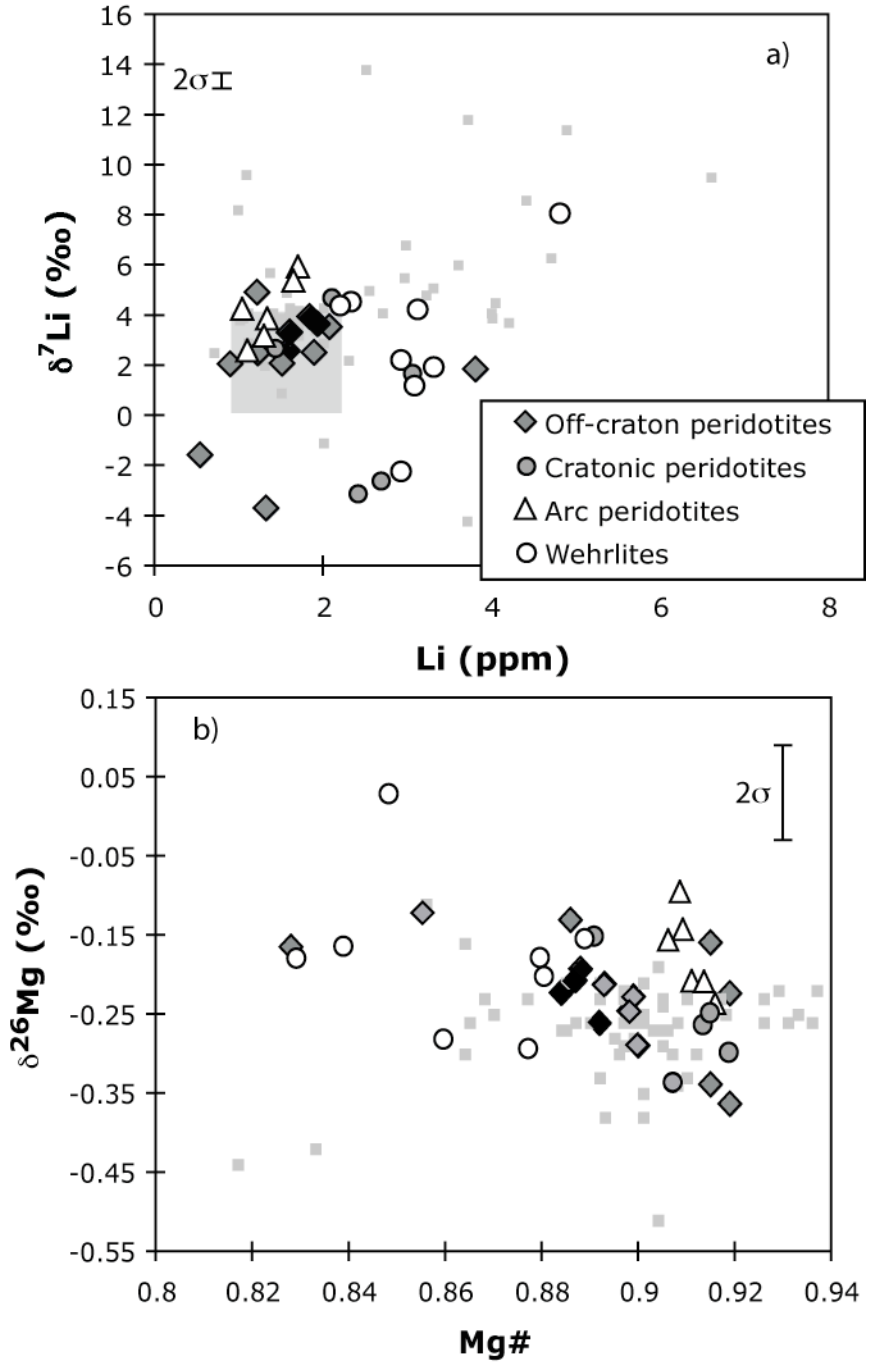

Figure 5

Figure 5

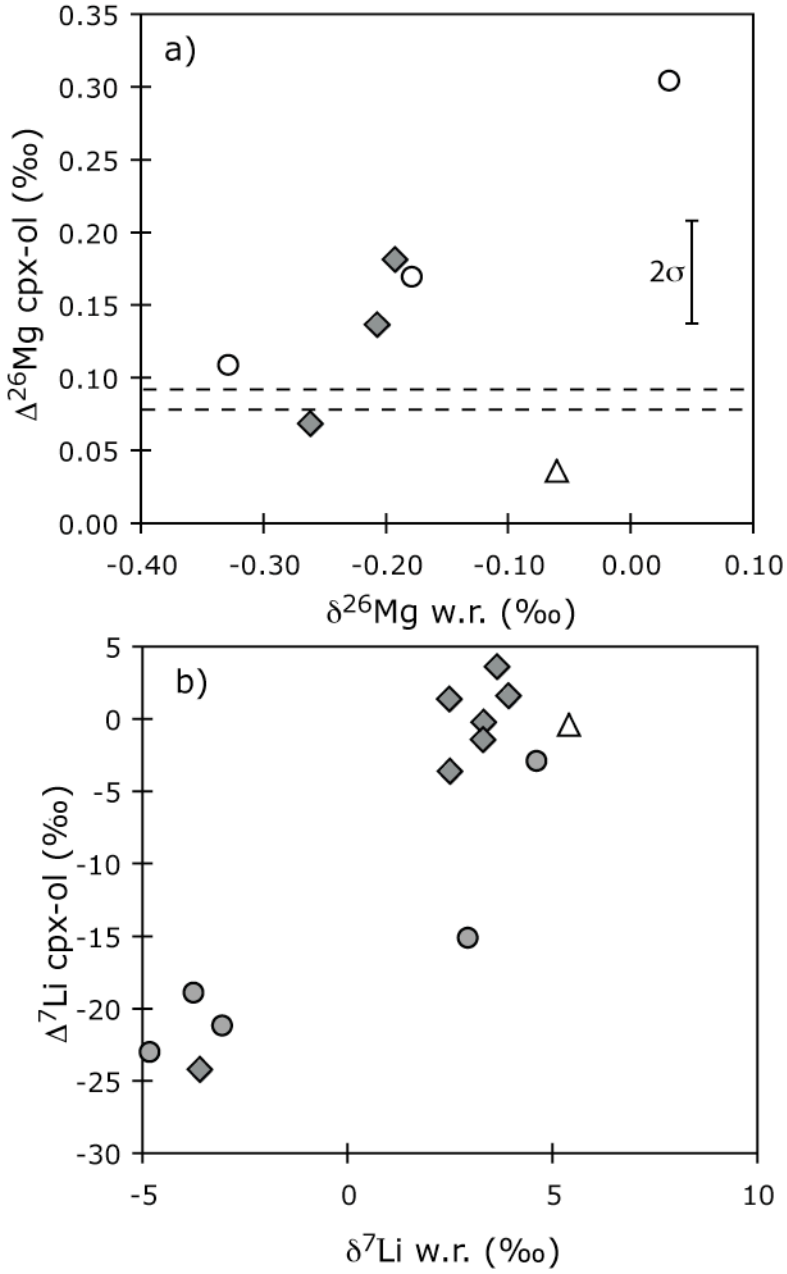
a)
0.35
0.30
0.25
0.20
0.15
0.10
0.05
0.00
Δ26Mg cpx-ol (‰)
2σ
-0.40
-0.30
-0.20
-0.10
0.00
0.10
δ26Mg w.r. (‰)
b)
5
0
-5
-10
-15
-20
-25
-30
Δ7Li cpx-ol (‰)
-5
0
5
10
δ7Li w.r. (‰)

Figure 6

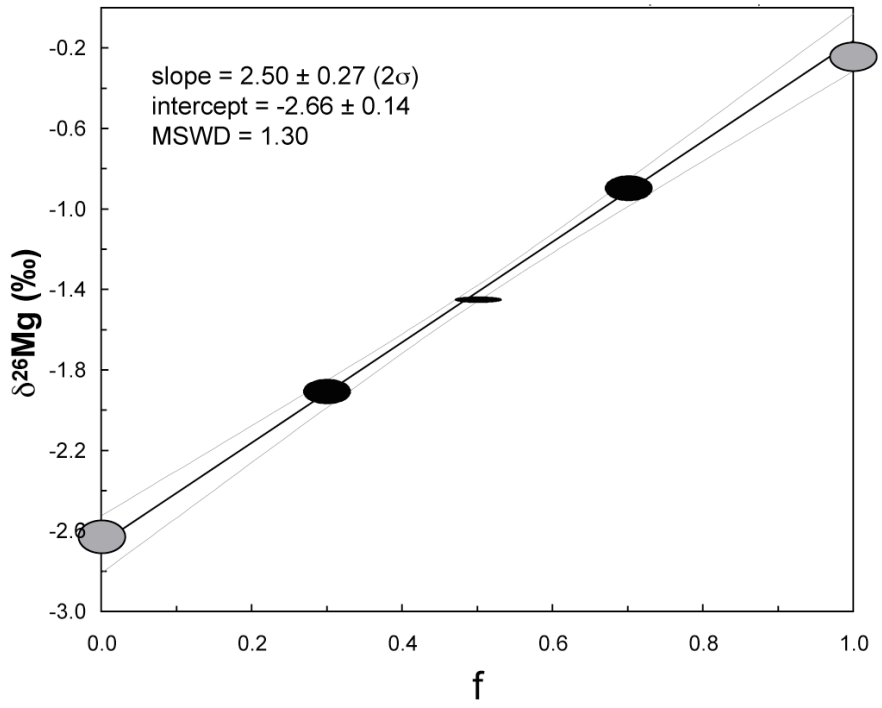

Figure 7

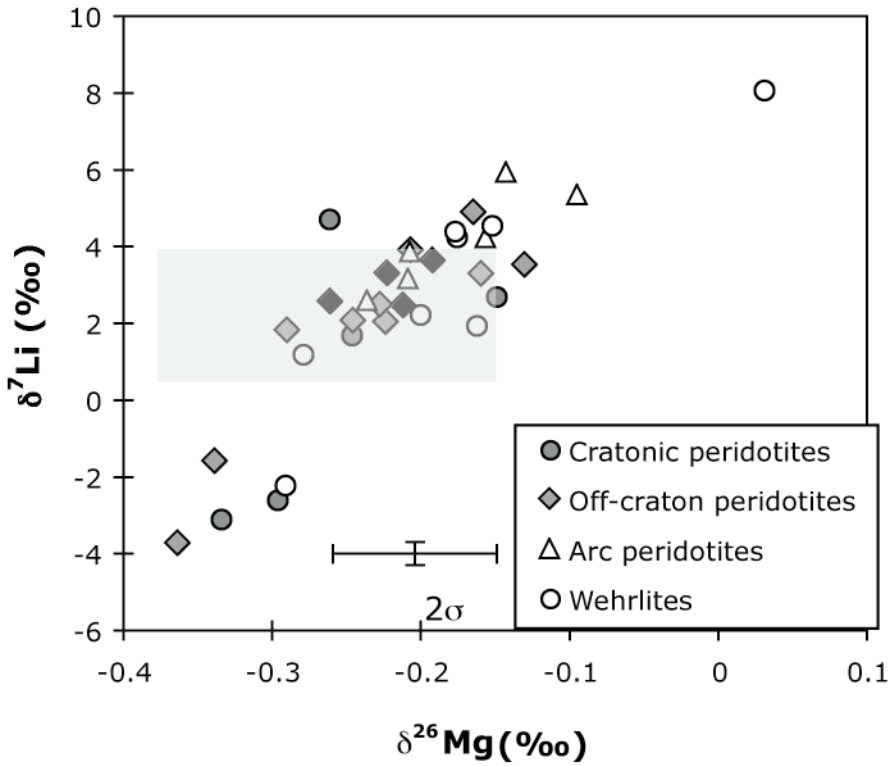

Figure 8

Figure 8

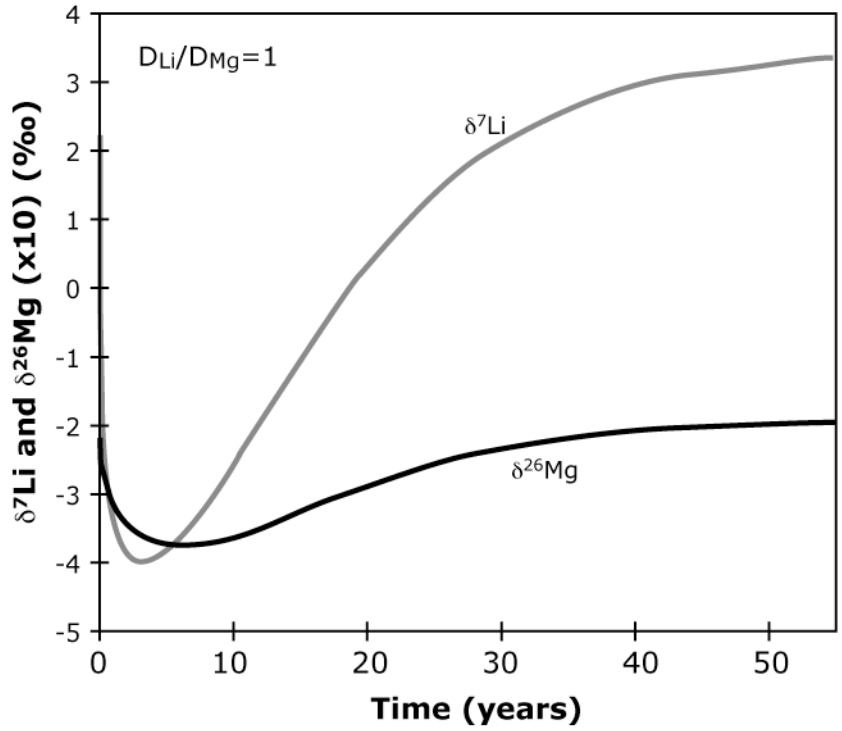

Figure 10

Figure 9

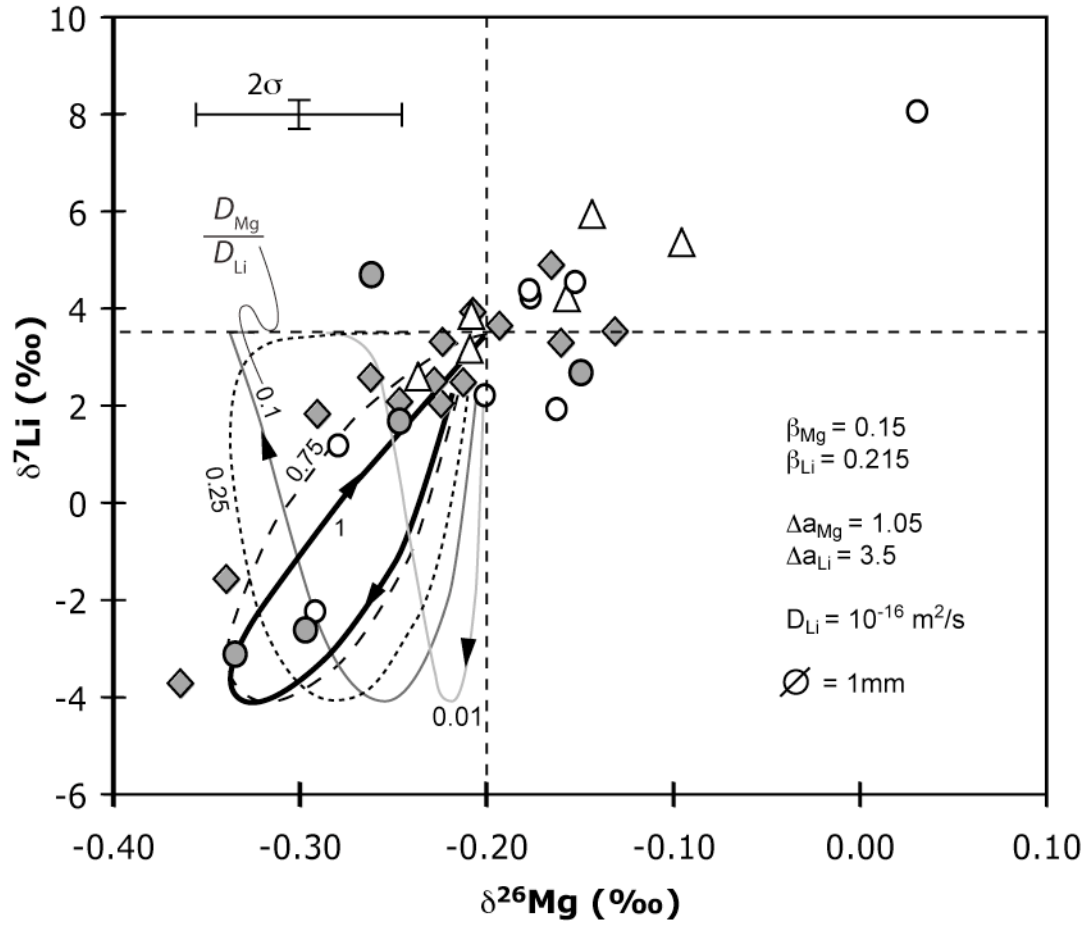

Figure 10

Figure 10

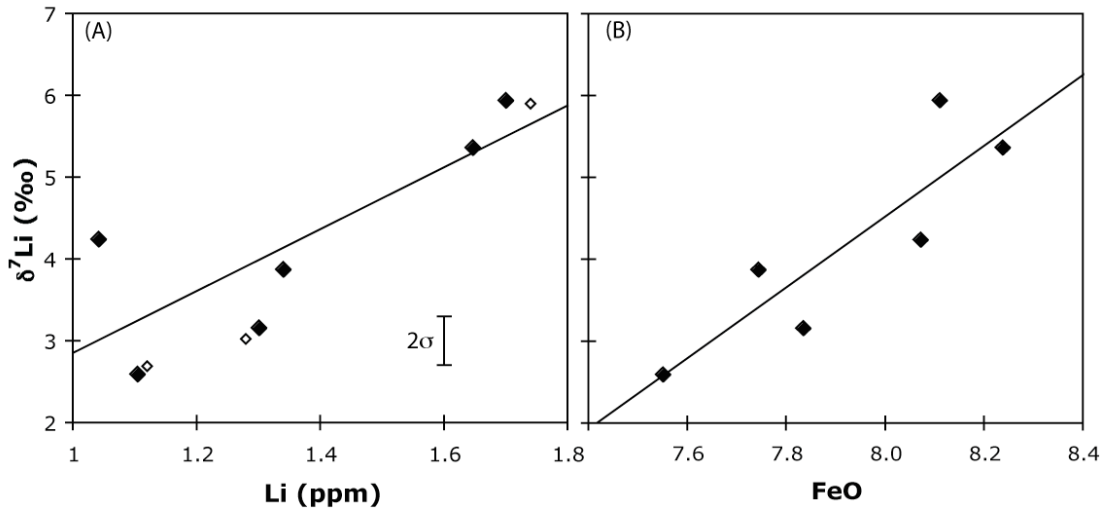

Figure 11